Global and Planetary Change 217 (2022) 103928

Contents lists available at ScienceDirect

Global and Planetary Change

journal homepage: www.elsevier.com/locate/gloplacha

Research paper

Did Schwabe cycles 19–24 influence the ENSO events, PDO, and AMO indexes in the Pacific and Atlantic Oceans?

Franklin Isaac Ormaza-González [a,*], María Esther Espinoza-Celi [a], Heydi Mariana Roa-López [b]

[a] ESPOL Polytechnic University, Escuela Superior Politécnica del Litoral, ESPOL (Facultad de Ingeniería Marítima, Ciencias del Mar), Campus Gustavo Galindo Km. 30.5 Vía Perimetral, P.O. Box 09-01-5863, Guayaquil, Ecuador

[b] ESPOL Polytechnic University, Escuela Superior Politécnica del Litoral, ESPOL (Faculty of Natural Sciencies and Mathematics). Campus Gustavo Galindo Km. 30.5 Vía Perimetral, P.O. Box 09-01-5863, Guayaquil, Ecuador.

ARTICLE INFO

Editor: Dr. Howard Falcon-Lang

Keywords:
Sunspots cycles
SST
SSTA
ONI
MEI
PDO
AMO
El Niño
La Niña
SOI

ABSTRACT

The sea surface temperature (SST), anomalies (SSTA), Oceanic Niño Index (ONI), and Multivariate ENSO (MEI) index in El Niño 1 + 2 and El Niño 3.4 regions, Pacific Decadal Oscillation (PDO) and Atlantic Multidecadal Oscillation (AMO), as well as the meteorological parameter Southern Oscillation Index (SOI) were cross correlated to sunspot counts (SS) from cycles 19 to 24 (1954–2019). Over the 1954–2019 period, the SS or Schwabe cycles did not show strong cross-correlation coefficients (cc-ρ) with values falling between 0.063 and 0.100 ($p < 0.05$). It seems that the Total Solar Irradiation (TSI) constant variability (±0.1%, ±1.361 W m^{-2}) due to the SS cycles balanced out throughout the whole period. The cc-ρ coefficients for SST and SSTA versus each individual SS cycles were between 0.100 and 0.200 with lag times between maxima of each being from a few to 48 months. The ONI showed a cc-ρ < 0.1, while MEI reached up to 0.2 through all SS cycles. The slope of the cc-ρ changed from negative to positive over 6–12 months periods, with peaks in slope change occurring somewhere between 2 and 3 years. The SOI cc-ρ varied by around 0.200 through cycles 19–21, but for SS 22–24 it was not noticeable. Interdecadal indexes PDO and AMO showed cc-ρ of up to 0.283; with a possible association of 8%, with a lag time of 1–3 years. During the ascending and descending phases of each SS cycle, the cc-ρ were 0.288 and − 0.233, respectively for SST in El Niño 3.4 region, but in El Niño 1 + 2 were negligible. The ONI and MEI showed cc-ρ up to 0.448 and 0.480 respectively with lag times of 1–15 months in ascending phase of the SS cycle. The SS vs SOI had cc- ρ up to +0.420 to −0.567 in the ascending phases, while PDO and AMO registered cc-ρ up to 0.417 and − 0.491. AMO appeared systematically associated with SS cycles from 10.0 to 30.2% during descending and ascending phases, respectively. Compiled SS counts for all the ascending and descending phases of the SS cycles, gave a clear spectral coherence (quasi sine-function distribution); for SST and SSTA, lag times of 9–48 months were observed with inverse and direct linear relationship, and peaks of −0.38 and 0.39, respectively. The ONI and MEI with SS counts have similar cc-ρ values: 0.245 and 0.387. Around 6–15% of the ONI and MEI can be explained by SS during ascending and < 4% in descending phases. It seems that over the relatively short time scales of SS cycles, either on their initial ascending or final descending phases, the studied indexes seem to be influenced. Even though it was difficult to elucidate the physics behind the observed cross-correlations, these results can be used to help improve understanding and aid the predictions of ENSO, PDO and AMO oceanographic events in the Pacific and Atlantic oceans.

1. Introduction

Essentially, the most important external source of energy to Earth is the sun. It has been determined this flux of energy can vary slightly in time. There are some solar cycles with markedly different periods (Ding et al., 2022) that affects the heat flux or solar constant reaching the Earth. Due to astronomical fluctuations of the Earth's orbit relative to the sun there is the predictable Milankovitch cycle with periods of tens to hundreds of thousands of years (Lindsey, 2009; Ding et al., 2022). The non-harmonic Suess or de Vries cycle spans 210 years due to variations of the cosmic ray-production (Suess, 1980; Raspopov et al., 2008). The Gleissberg cycles are 2–3 strong long cycles preceded by 2–3 weak ones

* Corresponding author.
E-mail address: formaza@espol.edu.ec (F.I. Ormaza-González).

https://doi.org/10.1016/j.gloplacha.2022.103928
Received 17 February 2022; Received in revised form 27 July 2022; Accepted 28 August 2022
Available online 3 September 2022

on time scales of around 105 years; since 1700 there has been 3 Gleissberg cycles (1700–1810, 1810–1910, 1910–2010, Dewitte et al., 2022; see also Peristykh and Damon, 2003; Peek, 2018). The Grand solar minimums (or Maunder Minimum) are periods where sunspot numbers are low or practically disappear over many decades, and the last occurred in 1645–1715. Within the human life timescale, the most important cycles are the sunspots cycles (Schwabe cycles), with a time span of just over 11 years (Hathaway, 2015). Fröhlich (2013) has suggested the magnetic Hale cycles that comprise two consecutives Schwabe cycles last around 22 years.

The above cycles affect the so-called solar constant, or the flux of energy at the upper atmosphere, which is about 1360 W m^{-2} (Hathaway, 2015) or 1.92 Ly day^{-1} (Ormaza-González and Sánchez, 1983). Kopp and Lean (2011) have reported that the most accurate accepted solar constant value is 1360.8 ± 0.5 W m^{-2}. Of this flux of energy, 50–75% reaches the Earth's surface (Ormaza-González and Sánchez, 1983; Lindsey, 2009) and the remainder is reflected and/or absorbed by clouds, particles, gases, etc. (Horning et al., 2003). About 90–93% of that energy reaching the surface is accumulated in the oceans (Trenberth et al., 2014; Clutz, 2017). The solar constant is affected by variations in sunspot number or counts (SS, Bhowmik and Nandy, 2018), and other solar activity parameters by around 0.1%, i.e., about 1.361 W m^{-2}. Sunspot cycles are characterized by increasing and then decreasing SS numbers (Hathaway, 2015). Fröhlich (2013) suggested that the solar constant can vary by up to 4.0 W m^{-2} over two SS cycles, i.e., a 22-year Hale cycle, and proposed a simple relationship between SS and the solar total irradiation constant (TSI), by assuming a direct relationship between the two.

$$TSI = 1353.6 + 0.089SS;\ \left(r^2 \text{ of } 0.71, 95\text{–}99\%\text{confidence}\right) \quad (1)$$

The surface-subsurface layers of the ocean that interact with the lower atmosphere alternately release and absorb heat energy. The work of Zhou and Tung (2010) reported the impact of the TSI on global SST over 150 years, finding signals of cooling and warming SSTs at the valley and peak of the SS cycles. Schlesinger and Ramankutty (1994) report a global cycle of 65–70 years for SST that is affected by greenhouse anthropogenic gases, sulphate aerosols and/or El Niño events, but they did not imply any external forcing such as the SS. There have been other studies on how solar radiation variability could affect temperature (Lean et al., 1995; Meehl et al., 2009; Tsonis et al., 2015); recently, Cheke et al. (2021) have studied those solar cycles of SS that would affect the El Nino Southern Oscillation (ENSO) indexes.

There are well known oceanic events that show periodicity with low or high frequencies: 25–30 and 3–7 years, respectively. These include the Pacific Decadal Oscillation (PDO, Mantua et al., 1997; Mantua and Hare, 2002; Zhang et al., 1997; Yim et al., 2013), Atlantic Multidecadal Oscillation (AMO, Enfield et al., 2001; Condron et al., 2005; Gray et al., 2010) and Interdecadal Pacific Oscillation (IPO, Henley et al., 2015), as well as El Niño (Busalacchi et al., 1983, see COAPS Library's: http://www.coaps.fsu.edu/lib/biblio/coaps-a.html) or La Niña (Yuan and Yan, 2012). During El Niño events, the surface and subsurface lose energy to the atmosphere and the opposite occurs during La Niña (Trenberth et al., 2014; Fasullo and Nerem, 2016); these events have a periodicity of 3–7 years. The Interdecadal oscillations have a series of impacts; e.g., the PDO gives rise to teleconnections between the tropic and mid-latitudes (Yoon and Yeh, 2010), and the effects include: 1) ocean heat content (Wang et al., 2017a, 2017b), 2) the lower and higher levels of the trophic chain including small pelagic fisheries (tuna and sardines; Ormaza-González et al., 2016a, 2016b), 3) biogeochemical air-sea CO_2 fluxes (McKinley et al., 2006), 4) the frequency of La Niña/El Niño (Newman et al., 2003). The interactions between decadal oscillations PDO/IPO and AMO may also affect ocean heat content (Chen and Tung, 2014). All these low and high frequency oceanographic events have a direct impact on local, regional, and global climate patterns, and there is growing evidence that the driving source of energy is the sun (Gray et al., 2010). Thus, Huo and Xiao (2016) have found a positive strong cross-correlation between El Niño 2015–2016 and SS, as well as with the El Niño Modoki Index. White et al. (1997) reported that heat anomalies produced by variable solar irradiance are stored in the upper ocean layer, driving SST changes of 0.01–0.03 K and 0.02–0.05 K on decadal and interdecadal periods, respectively. Zong et al. (2014) in their review of the impact of the 11-year SS cycle and multidecadal climate projections have found global SST variations of 0.08 ± 0.06 K and 0.14 ± 0.02 K during the 11- and 22-year Hale Cycles, combined with a response lag time of 1–2 years in relation to the SS (see also, Kristoufek, 2017). Liu et al. (2015) and Asma et al. (2019) have reported that effective solar radiation plays a role in the modulation of annual and decadal ENSO (El Niño and the Southern Oscillation) fluctuations. Also, Qian (2017) has found a direct influence of SS cycles (long time scale) on the ENSO in El Niño region 3 (5°S to 5°N, 150°W to 90°W) and SS from 1408 to 1978; equally, Hassan et al. (2016) have also reported comparable results using the Markov method. More recently, Leamon et al. (2021) have stressed the need of accounting for solar activity changes in short term climate variability. The influence of SS minimum counts has even reported to affect rain season in Central Europe (Laurenz et al., 2019) with a lag of 3–4 years. Yamakawa et al. (2016) have reported that solar impacts in terms of SS numbers not only affect the troposphere but also the sea surface, even though SS abundance is only a partial measure of solar activity (Scafetta, 2014). Thus, whatever affects the solar irradiation falling on the surface of the oceans, including volcanic eruptions (Fang et al., 2020), and cloudiness for example, it would affect the gain or loss of heat content of the oceans. The cited works tried to find the physical reasons for these connections, but they remained unknown or difficult to explain.

The impacts of events such as El Niño or La Niña are enormous for the global ocean surface and atmosphere, with subsequent dramatic impacts on the wellbeing of many countries including Ecuador, Perú, and Colombia (Glantz, 2001; Ormaza-González and Cedeño, 2017). Ideally, the accuracy of predictions of these events should be improved (Thomas, 2017), and thus a series of models are nowadays regularly run (see https://iri.columbia.edu/our-expertise/climate/forecasts/enso/current/, Tao et al., 2020, Chen et al., 2022). Hypothetically the outputs of the models would improve if the role of fluctuations of the sun's energy from the Schwabe cycles that affects the afore mentioned events, are better understood.

The work reported here investigates how fluctuations of sunspots over time (1954–2019) may cross-correlate with low and high frequency oceanic events such as the sea surface temperature (SST), anomalies (SSTA), Oceanographic El Niño Index (ONI), Multivariate ENSO Index (MEI), Southern Oscillation Index (SOI) in the central and east equatorial Pacific Ocean; and PDO, as well as on the AMO in the North Pacific and Atlantic basins. The hypothesis is that even small variations of the TSI can be reflected in these tele-connected indexes (Llanes-Cárdenas et al., 2020).

2. Material and methods

Sunspots have been observed and registered since ancient times; Chinese astronomers and Anaxagoras registered them centuries ago, and Galileo Galilei (1613) wrote letters about sunspots and even made drawings on their position. Vaquero (2007) reported that consistent registration of SS can be found as early as 1600. However, data on sea surface temperature have been measured consistently only since the 1950s, especially in the Central Pacific. Reconstructed data has been extrapolated back to early 1900s, but they can be biased or uncertain (Jones, 2017). Therefore, the time series from 1954 to 2019 of SS, PDO, AMO, SOI, ONI and MEI, as shown in the Fig. 1, were selected for this work. This period cover sunspots cycles 19–24.

Data for monthly sunspot number (SS) were taken from the Royal Observatory of Belgium, Brussels, World Data Center SILSO (http://www.sidc.be/silso/datafiles).

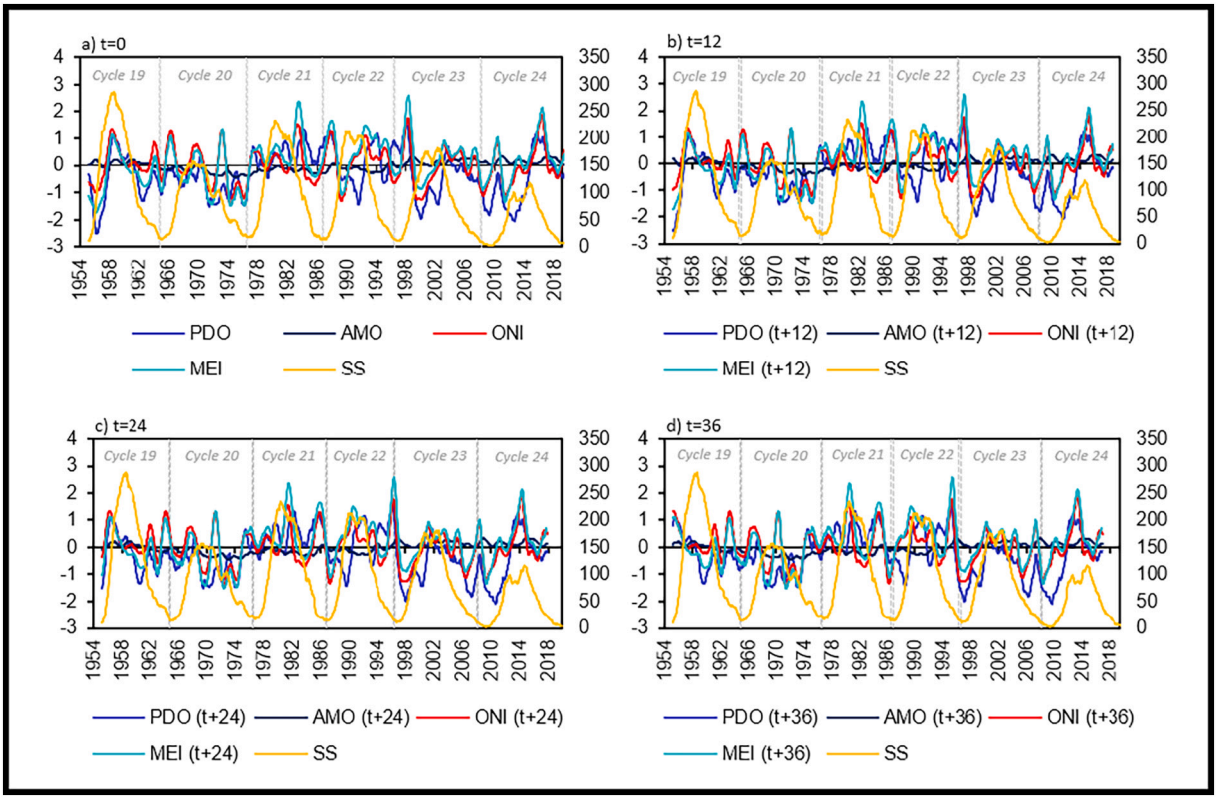

Fig. 1. Behaviour of monthly counts of SS, ONI, MEI, PDO and AMO. The Indexes start at $t = 0$, 12, 24 and 36 months (panels a, b, c, and d respectively). The SS series starts at t = 0 in the four panels. The left vertical axis gives the values for the Indexes, and SS counts at the right vertical scale. The end of each Schwabe cycle is marked by vertical dashed lines.

Data sources for other variables are given below. Note the the following geographic extents for El Niño areas: El Niño regions 3 + 4 (5°North-5°S, 170–120°W) and El Niño regions 1 + 2 (0–10°S, 90°W-80°W).

- Sea surface temperatures (SST) and SST Anomaly (SSTA): The Monthly Extended Reconstructed Sea Surface Temperature Version 4 (ERSSTv4, 1981–2010 base period). The Optimum Interpolation 1/4° Daily Sea Surface Temperature (OISST.v2, 1981–2010 base period), http://www.cpc.ncep.noaa.gov/data/indices/.
- Oceanic Niño Index (ONI): Huang et al., 2014): ERSST.v4 for El Niño/La Niña events since 1950 till December 2019: This index is the average of three sequential months of SSTA. http://www.cpc.ncep.noaa.gov/products/analysis_monitoring/ensostuff/ensoyears.shtml.
- Multivariate ENSO Index (MEI): This is a subsequent bi-monthly index that includes SST, sea level pressure, surface winds (meridional and zonal), surface air temperature and outgoing Long-wave Radiation (OLR_{500}) data (Wolter and Timlin, 1993, 1998, 2011; Zhang et al., 2019; Albert et al., 2022). https://www.esrl.noaa.gov/psd/enso/mei/table.html.
- Southern Oscillation Index (SOI). This monthly index follows large-scale fluctuations in air pressure occurring between the western and eastern tropical Pacific during high frequency events of El Niño and La Niña. (Climate Prediction Center - Southern Oscillation Index (noaa.gov), Rasmussen and Carpenter, 1982; Allan et al., 1991, Können et al., 1998; and Barnston, 2015)
- Pacific Decadal Oscillation (PDO): The PDO Index is based on NOAA's extended reconstruction of SSTs (ERSST Version 4) in the area: 20 N–65 N and 120E–100 W). It is constructed by regressing the ERSST Anomaly against the Mantua PDO Index for their overlap period, to compute a PDO regression map for the North Pacific ERSST Anomaly. The PDO Index closely follows the Mantua PDO Index at https://www.ncdc.noaa.gov/teleconnections/pdo/.
- Atlantic Multidecadal Oscillation is an Index of multidecadal SST centred on the North Atlantic Ocean between 20 N–65 N and 100 W–0E (d'Orgeville and Peltier, 2007). The data is accessible at: https://www.esrl.noaa.gov/psd/data/timeseries/AMO/

All Indexes have data from April 1954 to December 2019. The analysis was done using Excel and/or R statistical tools. The cross-correlation exercises were calculated using the complete series of SS solar cycles, and the SST Anomalies (in El Niño regions El Niño 3.4 region and El Niño 1 + 2 region), ONI, MEI, AMO, SOI and PDO Indexes. For the SS cycles 19–24 and their impact on the mentioned indexes, linear cross-correlations with monthly lags up to a maximum of 48 months, were conducted for:

1. the whole time series (1954–2019),
2. individual cycles,
3. ascendant/descendent phases of each SS cycle; and,
4. all ascendant and descendent phases of all cycles together.

2.1. Statistical approach

To determine if there was a relationship or association between sunspots and ENSO-oceanographic variables, the cross-correlation technique was used, since many of these associations may not occur at the same time between the analysed series but at a later or earlier time (Zhai, 2017). However, for the correct application of cross-correlation, it is necessary to have a "stationary" series, i.e., both, the means and variances of the series are independent of time (Brown, 1957). This is because, if they were time-dependent, the series would be

autocorrelated leading to the existence of a significant relationship between the series when in fact there is none, which is called "spurious correlation" (Jenkins and Watts, 1968). To avoid spurious correlations, it was ensured that the stationarity condition applied. When stationarity was not obtained in both chronological series, the differentiation process of the series was carried out to achieve this condition, and additionally in the cases of non-stationary series, as a precaution, the cointegration of the series was verified. (See Granger, 1986; Podobnik and Stanley, 2008, Tunnicliffe, 2016).

The cross-correlation was calculated through the formula (2)

$$\rho_{xy(k^+)} = \frac{1}{N}\sum\left[\left(\frac{X_t - \mu_X}{\sigma_X}\right) * \left(\frac{Y_{t+k} - \mu_Y}{\sigma_Y}\right)\right] \quad (2)$$

Where:

X_t is the value at time t of the independent stationary series

Y_{t+k} is the value at time $t + k$ of the dependent stationary series

μ_X, μ_Y, σ_X and σ_Y are the mean and standard deviation of X_t y Y_t respectively

As the time series was shown to be stationary, the relationships between sunspot variability and variations in oceanic indexes were investigated using time-lagged linear cross correlation relationships.

2.2. Statistical treatment of data

The time series of sunspot and ocean indexes were analysed for their stationarity condition through the Augmented Dickey-Fuller (ADF) test (see Sun et al., 2016). In cases where the series presented non-stationarity, it was identified whether the trend of the series was stochastic. Accordingly, the series was transformed with their first differences as indicated in formula 3a and 3b. However, in very few cases did we resort to the third difference of the series to obtain its stationarity.

$$L(X_t) = (X_t - X_{t-1}) \quad (3a)$$

$$L(Y_t) = (Y_t - Y_{t-1}) \quad (3b)$$

To proceed with the calculation of the cross-correlations of the series analysed, it was previously established whether to work with the original series or with the differentiated series that presented stationarity. Thus, in the case where the residuals of the regression between the SS series and each of the ENSO index series were stationary, i.e., the series were cointegrated, the cross-correlation was calculated using the original time series. In other cases, the calculation was made with the differentiated time series to ensure stationarity.

2.3. p-values and coefficients

The R statistical program provides the cross-correlation coefficients for each of the lags analysed. Additionally, confidence intervals of 90% and 95% were established for these coefficients with their respective p-values; those coefficients found to be statistically significant above 90% ($p < 0.10$) are presented (Lander, 1994).

The degree of cross-correlation (cc-ρ) in terms of Pearson coefficient is referred to as high, moderate, and low when the coefficient is between ±0.5 and ± 1.0, ±0.3 to ±0.49 and less than ±0.29 respectively (http://www.statisticssolutions.com/pearsons-cross-correlation-coefficient/). Even though the p values found for the reported r, were < 0.1, and there was high e consistency in the lag time for all the time-series for all indexes and regions, a due caveat must be exercised in interpreting the high or low cc-ρ reported. The degree of association (%) between the indexes and the SS was estimated by $(\text{cc-}\rho)^2 \times 100$. One of the main characteristics of this work is the use of oceanographic data from in situ measurements, and for that reason data before 1954 was not considered.

3. Results and discussion

Maxima in the PDO, AMO, ONI, and MEI series were offset by 0, 12, 24 and 36 months (Fig. 1, panels a, b, c, and d respectively), with the SS series starts at $t = 0$ in the four panels. It has been reported that the lag times for responses of some Indexes to SS cycles (SS) are around 12–36 months (see fig. 1 of Hassan et al., 2016), and Fang et al. (2020) have reported that ENSO responds with a 2–3 years of lag time after a major volcanic eruption. From 1954 to the present time, each sunspot cycle from 19 to 24 has occurred with a period of around 11 years (Hathaway, 2015), which is slightly less than the 11.2 years reported by Dicke (1978). The highest SS activity is seen in cycle 19 with around 250 SS/month, followed by <150, and at cycle 21 around 200, before decreasing steadily over cycles 22 to 24 to just over 100 SS/month. Cycle 24 is the lowest contemporary value of SS activity that is comparable only to cycles 12–15 (around 1880–1930) and is the lowest in the last 200 years (Clette et al., 2014). The negative or cold PDO phases (1947–1976, 2000-present) are within SS cycles 19–20 and 23–24, whilst cycles 21 and 22 are within the positive or warm phase of the PDO (1977–1999). As the PDO and AMO Indexes are displaced from 0 to 36 months on the time scale (Fig. 1), some peaks and troughs relative to SS activity can be seen. A cold phase of AMO was between the 1960s and 1990s, whilst the warm phase is from the 1990s to the present (McCarthy et al., 2015).

The ONI and MEI curves, both indicators of ENSO events, behave similarly throughout the study period (April 1954–December 2019), MEI has the highest anomaly peaks (> 2.0) when compared to ONI. In general, ONI and MEI curves indicate the highest positive anomalies between 1978 and 1995, a period that coincides with the warm and cold stages of PDO and AMO respectively (Maleski and Martinez, 2018). The highest peaks of MEI and ONI occur during the ascending and descending phases (period of increasing/decreasing number of sunspots) of the Schwabe cycles; that is, they never coincide directly with the maximum period of sunspots in the cycles, except in 1959 (Fig. 1, panel a). The two highest MEI peaks occur during the descending phase of solar cycle 21 and ascending phase of solar cycle 23. In mid-2016 both Indexes increased reaching the third highest peak of this period during the descending phase of SS 24.Conspicuous negative peaks (1953–1954, 1974–1975, 1999–2000, and 2010–2011) of these Indexes occurred on the low plateaus or just after the start of ascending phases of SS.

3.1. Whole series (1954–2019)

All variables (Fig. 2) were cross correlated with SS at lag times from 0 to 48 months over the six SS cycles. In general, at p-values of <0.10 and < 0.05, the spectral coherence from cross-correlation was low or poor, with cc-ρ varying between −0.063 and 0.100 with lag times between 3 and 46 months. In the ENSO area El Niño 1 + 2 region there was not a cross-correlation for SST, but for SSTA at lag 9 there was a positive cross-correlation of 0.066. In El Niño 3.4 region, SSTs correlated positively at lag 16 with cc-ρ of 0.066. Regarding the SSTAs in this region, negative cross-correlation was found at lags 46 (−0.080), and 16 (0.070). The index ONI did not show any cross-correlation during this period, but the MEI did at lag 21 (0.074). The SOI correlated with cc-p − 0.109 to +0.075 at lag time ranges of 30–48 months. The low-frequency indexes AMO and PDO have their highest correlation at lags 38 (0.088) and 4 (0.095) respectively. The response lags for AMO are in the range reported by Kristoufek (2017), who suggested a surface thermal response of around 24–36 months. The negative or positive cross-correlations would be a result of short-time variations of the indexes; for example, the PDO (https://www.ncdc.noaa.gov/teleconnections/pdo/) in 1954 it was −1.05 and 0.02 or in 1986, −0.3 and 1.00 in September and October, respectively. The small cc-ρ values, though statistically significant, mean sunspots would explain a correspondingly small fraction (0.4–1.0%) of these indexes.

The low cross-correlations found would support Lean et al. (1995), who suggested that since 1860, the increase of 0.25C can be attributed to direct solar forcing, according to their simple pre-industrial parameterization. On the other hand, Reid (2000) informed a TSI change of 1% in the last 400 years, whilst Kopp and Lean (2011) have reported a total

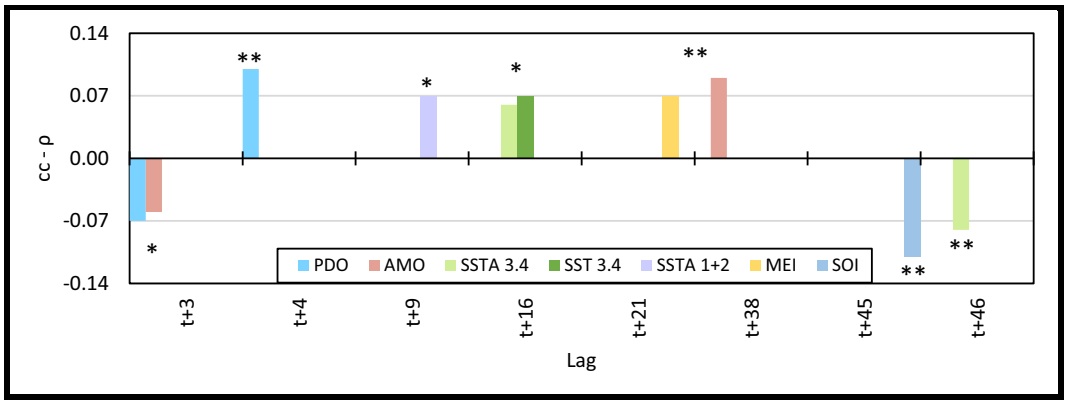

Fig. 2. Linear cross-correlations coefficients (cc-ρ, ***p*-values <0.05, **p*-values <0.1) between SS monthly counts and PDO, MEI, ONI, SOI, AMO, SST and SSTA in El Niño 1 + 2 region, and El Niño 3.4 region for the period April 1954 to December 2019 at different lag times. Negative cc-ρ means inverse linear cross-correlation.

solar irradiance (integrated overall wavelength spectrum) of around 0.1% over the last 30 years. More recently, Scafetta et al. (2019) reported that TSI had variations of 0.15–0.45 W m^{-2} in the period 1980–2018 that are based on direct satellites observations.

The TSI fluctuations are strongly correlated to SS (Hansen et al., 2013), the range of variation of 0.07% (Gray et al., 2010) lays around 1366 is ±0.95 W m^{-2}. This sort of variation may impact surface ocean heat content because 1) the total TSI integrates over all the wavelengths from UV to IR, and 2) the heat capacity (3.9 $J\ g^{-1}C^{-1}$) of the seawater is huge; an increase of 1C (24–25C) of 1000 kg of water requires 2 W/month. If a TSI of 0.24 W m^{-2} flows through the ocean surface for one month, the increase of SST would only be 0.12C in the first meter of the mixed layer, assuming neither loss nor gain due to external physical factors.

The relatively poor cc-ρ values can also be explained by how SS cycles are affected by internal processes in the sun, such as the hypothesized Minimum of Maunder (Eddy, 1976; Shindell et al., 2001; Ineson et al., 2015; Mörner, 2015; Le Mouël et al., 2019), which would be reflected on a global and regional basis. Lockwood (2010, 2013)), and Komitov and Kaftan (2013) argue that a grand solar minimum is coming as SS cycle 24 develops. There has not been a solar activity decline such as that found in SS 23–24 over the last 930 years, and such a solar minimum may last through cycles 24, 25, and 26 (Hady, 2013). Recently, Miyahara et al. (2021) reported that the Maunder Minimum would depend on how SS 25 will behave; this cycle started in May 2020 (Leamon et al., 2020).

3.2. Individual cycles

Cross-correlation analysis was split into individual SS cycles from 19 to 24. Almost no cross-correlation between SST and SS cycles was found, except in cycle 19 (Fig. 3). On the other hand, cc-ρ values observed for SSTA in both regions were from 0.157 up to 0.206, indicating a low but statistically significant cross-correlation (Fig. 3). The SSTA in El Niño 1 + 2 region appeared to be affected in all cycles except 22; with positive cc-ρ between 4 and 12 lags, only in SS cycles 21 and 23 showed negative cc-ρ. In general, the SSTAs in El Niño 3.4 region and El Niño 1 + 2 region were cross-correlated against almost every SS cycle and the slopes of the linear cross-correlation were basically positive in El Niño 3.4 region, with the highest cc-ρ for all cycles except SS 20. The SSTAs in El Niño 3.4 region had similar cc-ρ coefficients to those in region El Niño 1 + 2 region. The SSTA cross-correlation coefficients values were not better than 0.206 in both regions, with higher variability in El Niño 1 + 2 than El Niño 3.4 regions both in response time and cross-correlation coefficients (Fig. 3).

The magnitude of the SSTAs can slightly change depending on the reference used. There are 5 versions of ERSST (Huang et al., 2017) and currently, version 5 tends to be used in El Niño studies; here we used ERSSTv4 (Huang et al., 2014). Huang et al. (2017) stated that there is not a noticeable difference between ERSSTv4 and ERSSTv5. The negligible cross-correlation of SST and sunspots could be explained as the changes of the variability of SST is in the order of 0.5C, which is <2% of the SSTs readings, except during El Niño o La Niña. On the contrary, SSTAs fluctuations of 0.1C are around 20% of 0.5C anomalies; thus, it becomes more noticeable. The SSTAs values of +0.5C and − 0.5C are the boundaries for El Niño and La Niña; higher or lower these values define

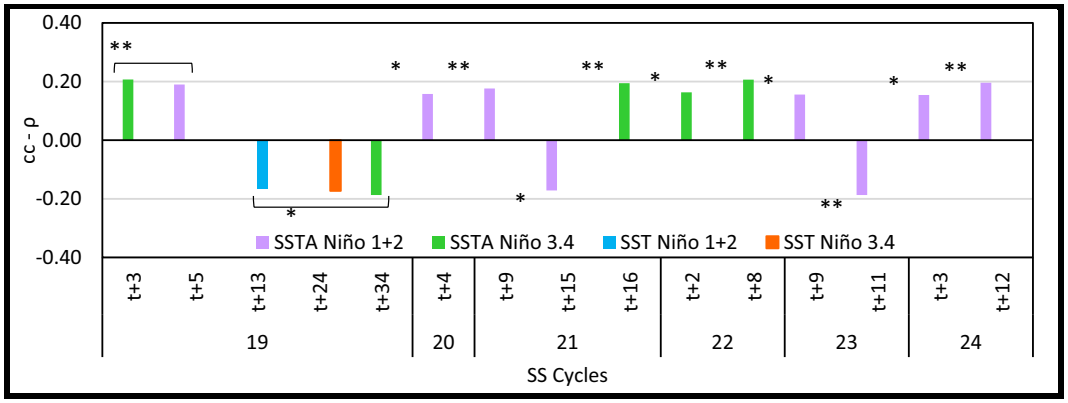

Fig. 3. Linear cross-correlation coefficients cc-ρ of SS monthly counts for individual cycles 19–24 against SST and SSTA in El Niño El Niño 1 + 2 and El Niño 3.4 regions. cc-ρ < 0.100 were removed in all graphs.

the events respectively.

Surface winds plus other coastal oceanographic and meteorological variables such as surface currents, upwelling, wind, cloudiness, water vapor, etc. could play an important role in this high variability. In El Niño 1 + 2 region, winds are not only generated in the local area but farther away, including the trade winds of the western Atlantic (Ormaza-González and Cedeño, 2017). Also, ENSO processes in the western Pacific could add variability in the SSTA in El Niño 3.4 region.

3.2.1. ONI and MEI

El Niño Index ONI (Fig. 4) showed low-poor spectral coherence (cc-ρ <0.1) with the SS cycles, except in 19 and 22 with cc-ρ coefficients of −0.167 (lag 25) and − 0.200 (lag 39) respectively. On the other hand, the MEI showed to be cross correlated throughout all the SS cycles with the highest positive coefficients of 0.173 (SS 19, lag 2), 0.181 (SS 20, lag 20), 0.209 (SS 21, lag 14), 0.254 (SS 24, lag 5), and negative coefficients −0.182 (SS 19, lag 28), −0.315 (SS 20, lag 12), −0.210 (SS 21, lag 14), and − 0.215 (SS 22, lag 5). Overall, the linear cross-correlation averaged 0.204 and − 0.230. The lag time for both indexes varied amply, the positive mainly occurred within the first 6 months, and the negative within the year; however, cross-correlation was also determined in the period 27–38 months. Huo and Xiao (2016) found strong a cross-correlation between SS and El Niño Modoki during 2015 (SS 24). Zhai (2017) also has found a cross-correlation of −0.109 between El Niño/Southern Oscillation (ENSO) and SS in El Niño 3 region (5°S ~ 5°N, 150°W ~ 90°W), which can be considered as a thermal transition zone between regions El Niño 1 + 2 and El Niño 3.4.

The variability of the slope in cross-correlations could arise from: 1) SS numbers showing large variations from 1 month to another, 2) regional meteorological conditions (particularly cloudiness), ocean surface currents that exchange heat in/out region El Niño 3.4 region, 3) equatorial Kelvin waves (Gill, 1982; Webb et al., 2020), 4) the fluctuation of the SOI index (http://www.cpc.ncep.noaa.gov/data/indices/soi), 5) volcanic eruptions (Fang et al., 2020), and 6) the reference period for ONI, which changes every 5 years (Lindsey, 2013). The most recent ONIs (v4 or v5) are supposed to be better and more consistent as data acquisition improves. On top, the ONI has a variable reference period of 30 years; thus for 1950 to 1955 the reference period is 1936–1965; for 1956–1960; 1941–1970, etc. This could produce variability on this index affecting the cross-correlation with SS. From the statistical point of view, the variability of the correlations (sometimes positive or negative) could be a reason why cc-ρ are small for the entire time interval. In the referred work of Huo and Xiao (2016) using reconstructed time series found a cross correlation of around 0.1, while here with actual acquired data of the indexes the cc-ρ is averaging 0.204 and −0.230.

Regarding MEI, this additional Index for El Niño events had higher cross-correlation coefficients than ONI across the six cycles, but with rapid changes of the slope signal, which could be attributed to the differences between these indexes.

1. The ONI is established by the SSTAs in El Niño 3.4 region, while the MEI combines five oceanographic and meteorological variables, which are: sea-level pressure (SLP), sea surface temperature (SST), zonal and meridional components of the surface wind, and outgoing longwave radiation (OLR)) over the tropical Pacific basin (30°S–30°N and 100°E–70°W, https://psl.noaa.gov/enso/mei/).
2. Atmospheric variability: Zhang et al. (2019) have discussed how atmospheric noise can affect important uncertainties when coupled ENSO models are analysed; thus, it is plausible to argument this noise is affecting the slope variability of the cross-correlations coefficients.

Therefore, the better cross-correlation found with the MEI than with the ONI, could be mainly explained in terms of these differences mentioned above.

3.2.2. PDO

This interdecadal Index (Fig. 4) had cc-ρ coefficients ranging from 0.240 (SS 21, lag 24) to −0.282 (SS 24, lag 9). The correlations were mainly negative in cycles 19 (lag 9) and 20 (lag 14); then, positive 21 and 22 and again negative in 23 and 24. These coefficients would suggest an influence of SS over the PDO would be up to 8%, and the signal of them would be in synchrony with the cold (1954–1978, 2000-present) and warm (1979–1999) phases of the PDO.

3.2.3. AMO

This inter-decadal index (Schlesinger and Ramankutty, 1994; Kerr, 2000; d'Orgeville and Peltier, 2007; Li et al., 2016) for the North Atlantic basin registered higher cross-correlation with cc-ρ >0.100 through all cycles than its sister index PDO of the Pacific. The Fig. 4 shows the highest positive (0.235) and negative (−0.281) coefficients ($p < 0.05$). Up to 8% of the AMO signal could be ascribed to SS at some moment between 1 and 30 months, but mainly in the lower range (<10 months). Another study as the one from Gray et al. (2016), has reported lag time responses of mean-sea-level pressure over the Atlantic to SS cycles of 36–48 months over a longer time series study of 32 solar cycles.

It can be observed from Fig. 4 that generally PDO and AMO correlations seem to alternate; Li et al. (2016) reported these indexes are in quasi opposite phase. This coincides with the phases of the AMO, positive 1930–1965 (SS 19), negative from around 1965 to 1998 (SS 20–22), and positive from 1998-present (SS 23–24), see http://appinsys.com/globalwarming/amo.htm. It is noteworthy to observe that the cross-correlation slopes of the PDO and AMO are opposite respectively during the cycles 19, 20, and 23 (cold phase PDO), but in concordance in

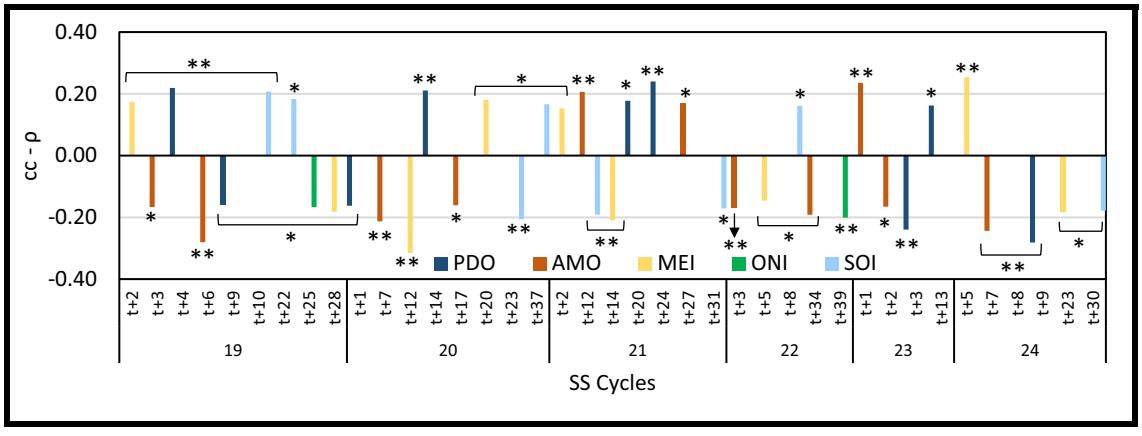

Fig. 4. Linear cross-correlation coefficients cc-ρ of SS monthly counts cycles 19–24 against PDO, AMO, MEI, ONI, and SOI Indexes.

cycles 21 and 24, but in cycle 22, PDO does not cross-correlate to SS at cc-ρ >0.100. d'Orgeville and Peltier (2007) have shown that PDO and AMO are correlated one to another with a lag time of about 13 years, which is closed to one Schwabe cycle period.

3.3. Ascending and descending phases of solar cycles

As the SS cycles are best cross-correlated to the variables studied on a response time from 2 to 36 months, there was the need to study their influence during the ascending and descending phases, which have >50 and- >66 months each (see Fig. 1).

The SST the regions El Niño 3.4 and El Niño 1 + 2 presented cc-ρ coefficients >0.15 during the descending phase of the SS cycles 19, 20, and 22, with negative slope. The highest coefficients were + 0.288 and − 0.233 in El Niño 3.4 region during the ascending and declining phases, respectively. Thus, the influence of the SS cycles could reach 8.3% on the SSTs values, but they are more susceptible during descending phases, especially in those cycles which have the highest SS counts in the analysed series, therefore with the highest change of TSI. In El Niño 3.4 region the SSTs response was much clearer than for El Niño 1 + 2 region, as in the later there is influence on coastal processes were waves, tides, coastal surface currents upwellings, winds, interactions between the Humboldt and Panama Bay water masses, as well as variable changes in cloudiness, rain, etc. These conditions and variability can produce dramatic impacts of the SSTs in short scale, producing El Niño Costero (Ramírez and Briones, 2017; Song et al., 2021), or rapid and short sea surface coastal warming (Ormaza-González and Cedeño, 2017; Lübbecke et al., 2019). Even rapid cooling, due to pulses of the Humboldt current (Montecino and Lange, 2009), like the one registered in mid-March 2021 (Ormaza-González, 2021) or more recently February 2022 (https://twitter.com/FranklinOrmaza1/status/1494308514034032640). All these factors would be enlarged or mask the SS signals in El Niño 1 + 2 region.

The SSTA (Fig. 5a/b) in El Niño 1 + 2 region cross-correlated with SS many times, especially during descending phases of all cycles except SS 22 with cc-ρ up 0.389 (SS 24) and main lag times from 5 to 13 months. The SS cycles (20 and 24) during cold phase PDO showed alternate cross-correlation reaching a maximum 0.389 and negative −0.314 ($p < 0.05$). During the ascending phase in El Niño 1 + 2 region (blue bars, Fig. 5a) the cc-ρ peaked at 0.393 ($p < 0.05$). In the cycles 19 and 24 the highest cc-ρ were found, −0.460 and 0.394 ($p < 0.05$) respectively. These coefficients coincided with the largest (over 2 years) and most intense (<−1.5C) La Niña during 1954–1955, and 2010–2012 (Fig. 12). It must be noticed that during cycle 21 two big events El Niño (1983–1985) and La Niña (1984–1985) were registered as well as in cycles 23 and 24 with coefficients just around 0.2. The highest coefficients would mean an influence up to 21.2% and 15.5% of the SS on the SSTAs in El Niño 3.4 region. These results would suggest the cross-correlations are stronger in El Niño 3.4 region due to the less dispersing oceanographic-meteorological conditions than in El Niño 1 + 2 region. Also, these findings would suggest that during the cold phase of PDOs (see NOAA, 2016), the cc-ρ in El Niño 3.4 region tends to be higher, as the solar energy reaching the ocean surface increases as the cloudiness tend to decrease significantly during prolonged periods around or over in El Niño 3.4 region (Porch et al., 2006).

3.3.1. The ONI Index

There was not a clear spectral coherence of the ONI during the declining phases (Fig. 6); only in cycle 19 (lag 25) and 20 (lag 12) registered cc-ρ ($p < 0.10$) of −0.222 and − 0.196 respectively, but in the ascending phases of cycle 21, period of two big El Niño and La Niña, the coefficient had a clear pattern from lags 1 to 15 months reaching to 0.448 ($p < 0.05$, lag 15) which is the highest coefficient found, implying a possible SS influence of up to 20.1% and 4.9% during ascending and descending SS phases respectively (see Fig. 6). The ONI cross-correlations were not in accordance with what was found with SSTA

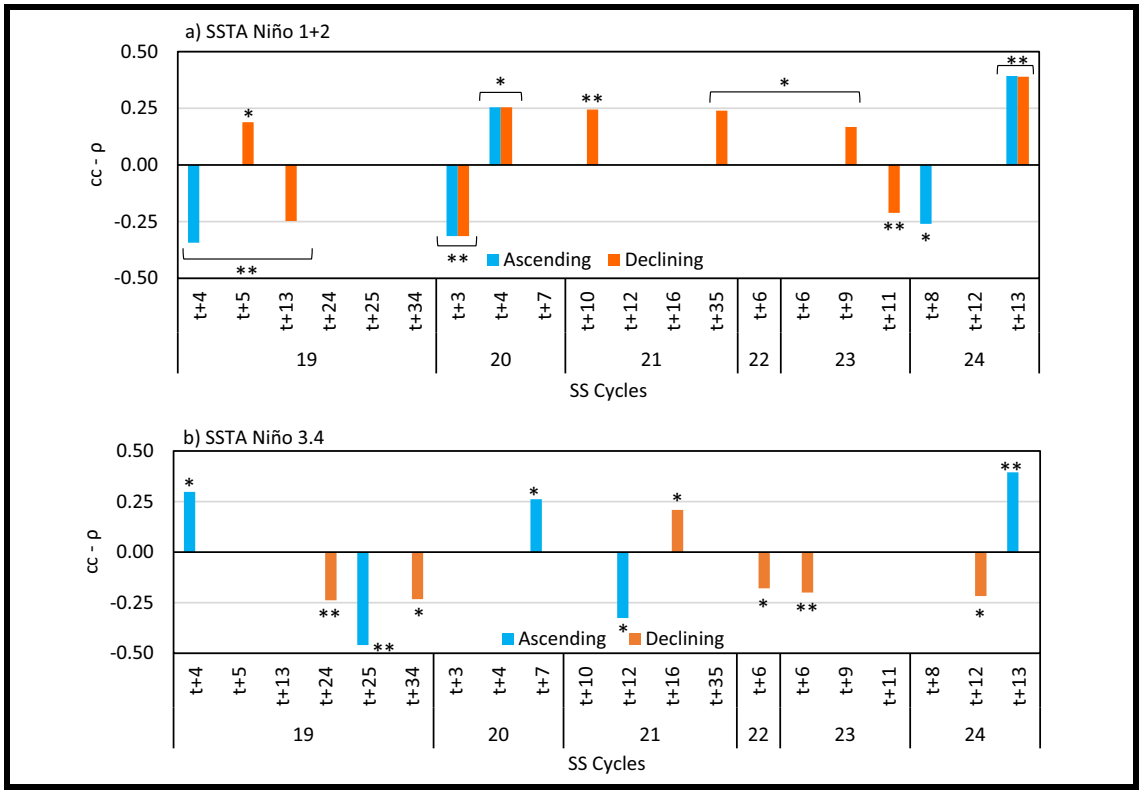

Fig. 5. Linear cross-correlation coefficient cc-ρ of SS monthly counts during the ascending (blue) and declining (red) phases for SS cycles 19–24. a) SSTA in El Niño 1 + 2, and b) SSTA in El Niño 3.4 regions. (For interpretation of the references to colour in this figure legend, the reader is referred to the web version of this article.)

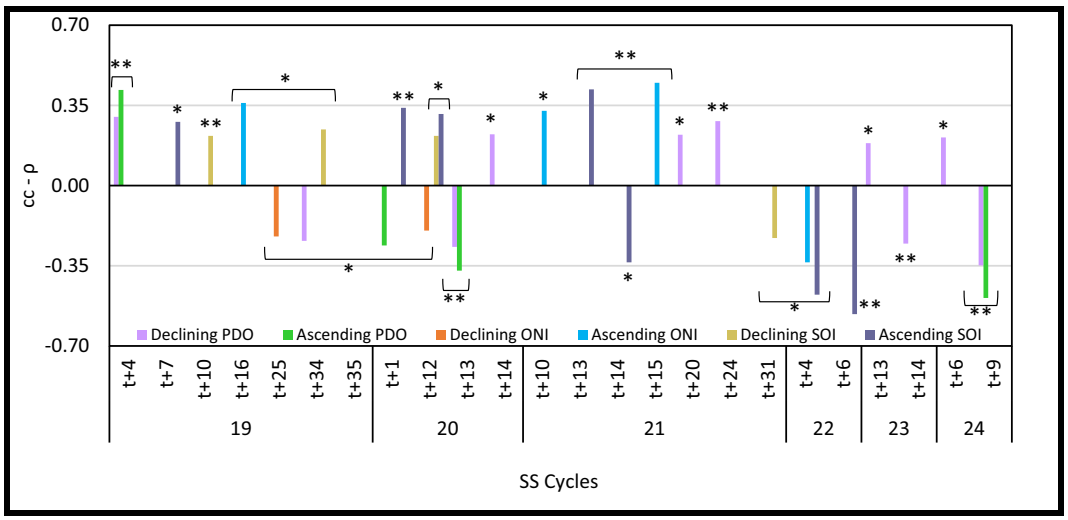

Fig. 6. Linear cross-correlation coefficient cc-ρ of SS monthly counts during the ascending and declining phases of SS cycles (19–24) against ONI, SOI and PDO-.

in El Niño 3.4 region, the main reason is that ONI measures the average of three consecutive months, while SSTA is just the monthly average of daily measurements as well as the sunspots counts.

The atmospheric ENSO index SOI, showed to be correlated with cc-ρ from 0.200 (SS 20, lag 31) up to 0.567 (SS 22, lag 15) that shows the SOI could be explained up to 32.1% by the SS during ascending phases, whilst for the descending phase cc-ρ was lower (0.092 to 0.200).

3.3.2. The MEI Index

The Multivariate ENSO Index does not only consider the SST Anomaly but also sea-level pressure and other variables (Allan and Ansell, 2006; Wolter and Timlin, 1998). The MEI correlated in all ascending and descending phases of SS cycles (Fig. 7). During the ascending phase, it was notorious in SS 19 the highest cc-ρ of 0.480 (lag 6); in general, the cc-ρ was >0.270, thus the influence of SS counts would be in the range of 7.3 to 23.0% at some moments of this phase. The SSTA and ONI also showed moderate cross-correlation coefficients (±0.3 to ±0.49) during this cycle, which in turn has the highest SS monthly counts (>280 SS) rendering the highest change of TSI in the studied period. The sun cycle 19 is the most intense since the last 100 years, the contrary is the cycle 24 (NWS, 2021). In general, the ascending phase of the SS cycles takes a shorter time than descending phase, therefore the slope of the curve is steeper (Fig. 12); then the increasing change of the TSI influences in a clearer way the studied indexes. It seems that during the ascending phases, El Niño events are prone to develop as TSI increases (as well as UV radiation does, NWS, 2021), while during plunging SS phases, when the TSI tends to diminish (see Formula (1)), could lead to La Niña events, like the 2020–2022 occurrence (Ormaza-González, 2021). In a more detailed view, warm events tend to occur in both; at the beginning and after the valley or peak of the cycle and have a variable delay time up to 24–36 months, which is within to the findings of Huo and Xiao (2016). The delay time is due to the slow heating/cooling by the TSI fluctuations over time in surface oceanic waters. However, this heating is also affected by others oceanographic and atmospheric parameters mention above. The descending phase of the cycles has a softer slope than the ascending phase, but a quicker response (0–12 months) of the ocean surface SST and ONI/MEI that could trigger neutral or cold events more cogently. Most of the La Niña events occur during the descending phase or just when approaching or leaving the valley or minimum SS counts (Fig. 12) when the TSI decreases and reaches the minimum (Scafetta et al., 2019). La Niña 2020–2022 is a good example, the lowest SS counts (<2 counts/months) occurred during extended periods when reaching the valley of the SS 24. The valley of SS 24 has had an extended period of close to 3 years, during which there have been weeks and months without sunspots, before the SS 25 started in December 2020 (NASA, 2021a, 2021b; Pishkalo, 2021).

The weakest sunspot cycle (SS 24) over the last 100 years (NWS, 2021) has had four La Niña events: 2007–2009, 2010–2012, 2016–2017, and 2020–2022 (Fig. 12), it is the only cycle with that number of La Niña events. A plausible reason is that during this cycle the number of sunspots (i.e., sun activity) is one the lowest, it has the 4th smallest intensity since Cycle 1 (1755) reaching only to 114 sunspots (of an average of 179), so it is the weakest cycle in the last two centuries (Clette et al.,

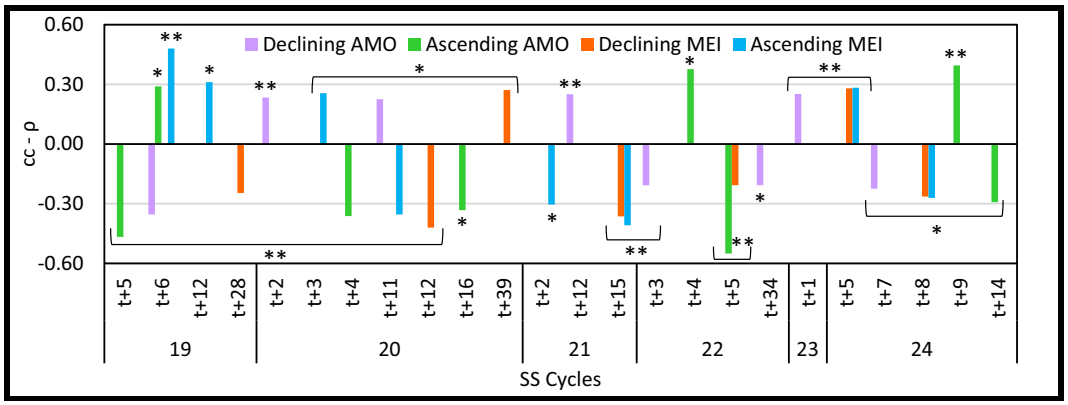

Fig. 7. Linear cross-correlation coefficient cc-ρ of SS monthly counts during the ascending and declining phases of SS cycles (19–24) against MEI and AMO.

2014); therefore, less energy has hit the ocean surface allowing a cooling effect during the last 12 years. Recently, Leamon et al. (2021) have reported that solar activity (measured by sunspots) affects the ENSO indexes, producing La Niña event at the end of the Hale cycles (22 years) or by the culmination of a descending phases. Three important exceptions are La Niña 1988–1989, 1998–2002, and 2010–2012 that are registered during cycles 22–24 during the rising phase (Fig. 11).

3.3.3. PDO

The Pacific Decadal oscillation gave positive and negative linear slopes during the descending phases of all cycles except SS 22 (Fig. 6), while during the ascending phases cross-correlation ($p < 0.100$) was observed in SS 19, SS 20, and SS 24. Cross-correlation coefficients up to 0.417 (lag 4) and − 0.491 (lag 9) were notorious SS 19 (Apr/54-Nov/58), and SS 24 (Jan/08-Feb/14) respectively during ascending phases, while for the descending phase in SS 24 the highest cc-ρ was found (−0.348, lag 9), and the main lag times were between 1 and 24 months. Huo and Xiao (2016) and Xiao et al. (2017) have reported that at interdecadal scale, the variations of solar energy, on indexes such as the PDO, could be more detectable in wide-open areas like Tropical Pacific, even though the complexity of the sea and atmosphere relationship response to solar energy input. These authors suggest that solar energy variation can even modulate El Niño Modoki, which is another oceanographic expression of El Niño (Ashok et al., 2007; Ormaza-González, 2016). The variation of solar energy due to sunspots on long time scales, yet with very weak changes, could produce decadal and millennial timescale impacts on global thermohaline circulation that in turn affect heat distribution (Bond et al., 2001, van Loon et al., 2007, Gray et al., 2013). The PDO, according to these linear cross-correlations could have been affected up to 24.1% by sunspots with a cc-ρ reaching the boundaries of 0.500, which in turn is the lower limit of a high cross-correlation coefficient.

3.3.4. AMO

During the ascending phases, moderate cc-ρ coefficients, between SS and AMO (Fig. 7) was found with values over 0.27 in all cycles except 21 and 23, whereas the cycles 19 and 22 showed higher spectral coherence than the others (Fig. 7), with cc-ρ values −0.467 and − 0.550 respectively in the range of moderate and high cross-correlation. In general, the slopes of the linear cross-correlations were highly variable. During descending phases cross-correlations were found in all cycles, the highest spectral density was in SS 19 and 20, with the highest coefficient of 0.354 in SS 19; the influence of the SS on AMO could account up to 30.2%. There is a certain opposite cross-correlation behaviour between PDO and AMO; somehow while the latter presented a lower spectral density in the declining phase, the first presents the highest on ascending phase. The results found could be explained as the AMO is in the opposite phase to the PDO (Enfield et al., 2001; Condron et al., 2005); i.e., warm in periods 1930–1964 and 2000-present (cold PDO), and cold in 1965–1999 (warm PDO). An explanation of this would probably be the different size of their geographical basins, the thermohaline circulation, and continental weather interaction. The PDO and AMO are inter-decadal cycles of 25–30 years, therefore during the ascending and descending of SS phases (i.e., increasing/decreasing TSI values) they would be strengthened or weakened, as shown by the linear cross-correlations.

A further exercise was compiling all ascending and descending phases of all cycles in one series each, which gave a longer phase scale than individual cycles. There was a clear correlation of the Schwabe ascending and descending phases in all indexes. During the ascending phase, the SST in El Niño 1 + 2 and El Niño 3.4 regions (Fig. 8a/b) showed cc-ρ from <0.1 to 0.350; the variability of the spectral coherence is high in El Niño 1 + 2 region while in El Niño 3.4 region the spectral coherence function resembles a sine function with a maximum cc-ρ of −0.35 (lag 8) and + 0.28 (lag 40). During the downward phase (Fig. 9a/b); the spectral coherence of the cross-correlations showed different fluctuations, SST in El Niño 1 + 2 region showed a less variable response

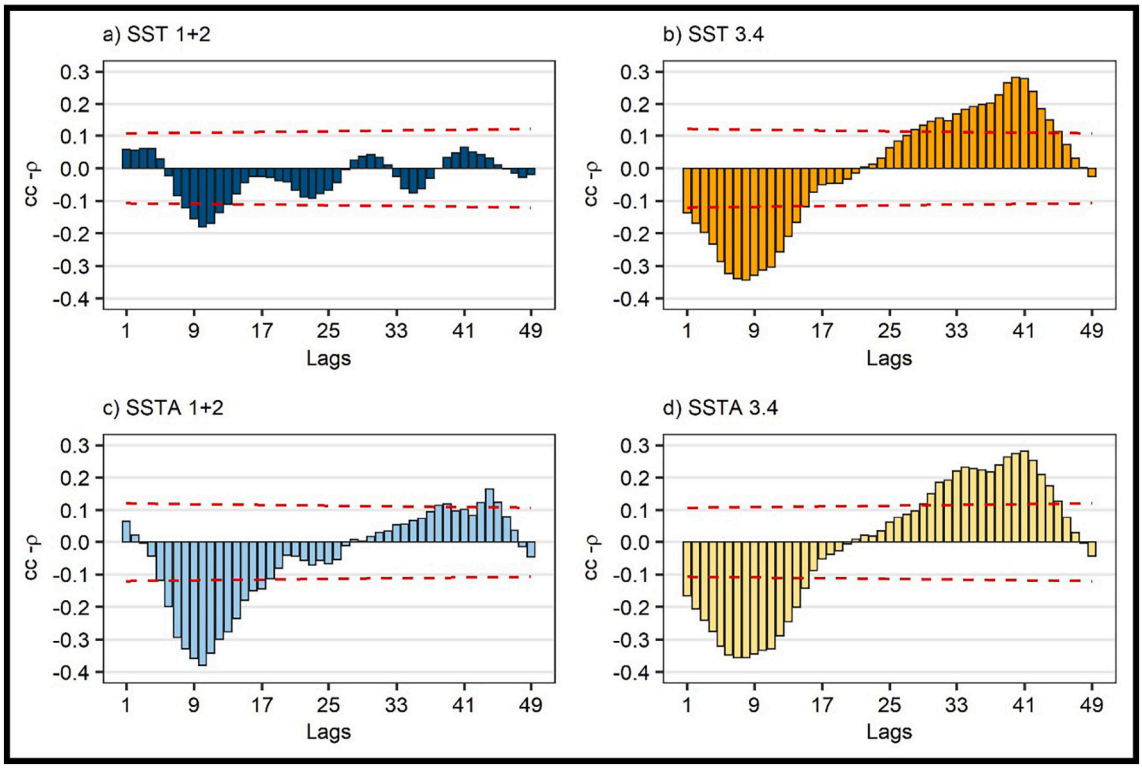

Fig. 8. Linear cross-correlation cc-ρ for all ascending phases of SS cycles agaisnt SST and SSTA in El Niño 1 + 2 and El Niño 3.4 regions. Panels: a) SST in El Niño 1 + 2 region; b) SST in El Niño 3.4 region; c) SSTA in El Niño 1 + 2 region, d) SSTA in El Niño 3.4 region.

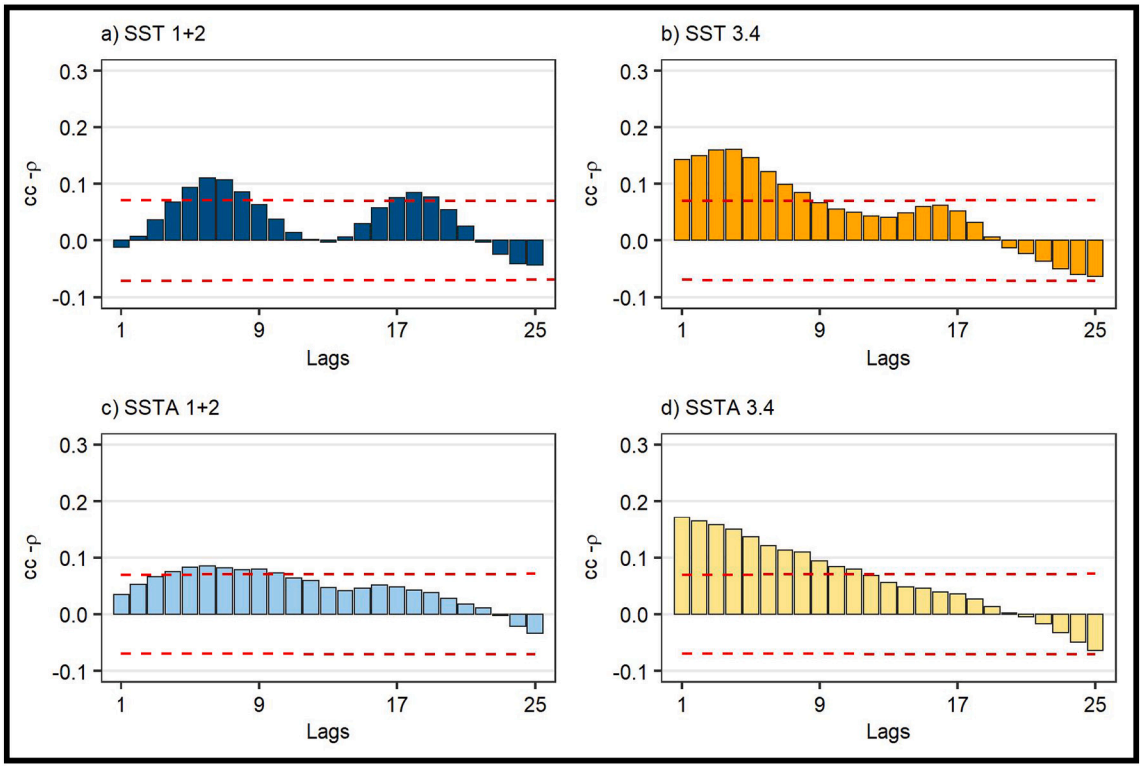

Fig. 9. Linear cross-correlation cc-ρ for all descending phases of SS cycles agaisnt: a) SST in El Niño 1 + 2 region; b) SST in El Niño 3.4 region; c) SSTA in El Niño 1 + 2 region, d) SSTA El Niño 3.4 region.

than in the rising phase. The cc-ρ were up to 0.10–0.15 (1% to 2.2%) in the descending but in the ascending from −0.35 to 0.28 (12.2% to 7.8%).

During the ascending phases, the SSTA in El Niño 1 + 2 and El Niño 3.4 regions (Fig. 8c/d), the spectral coherence was stronger and less noise showing resemblance of a sine curve with a minimum of −0.4 to maximum of >0.15 at lags 10 and 44 respectively, while in El Niño 3.4 region the values were 0.35 and 0.29 at lags 7 and 40 months in the same

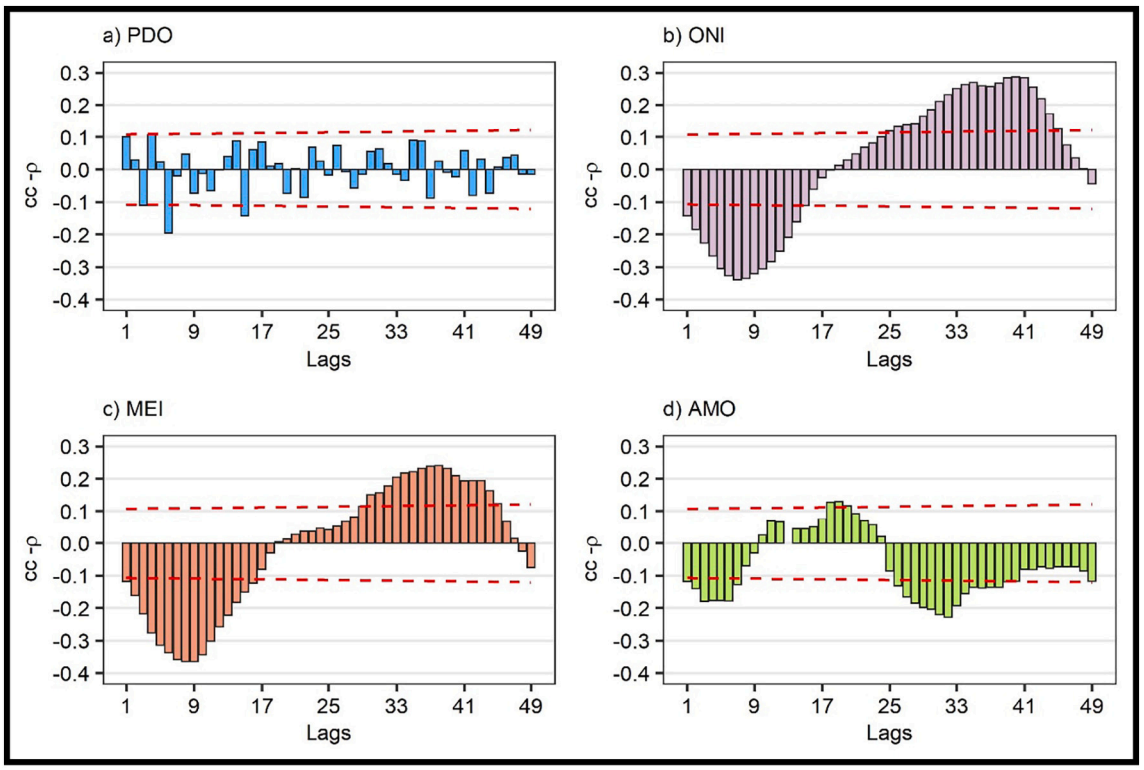

Fig. 10. Linear cross-correlation cc-ρ for all ascending phases of SS cycles agaisnt: a) PDO; b) ONI, c) MEI, and d) AMO.

order. Throughout the descending phases were similar in both regions (Fig. 9c/d) with a negative cc-ρ (around 0.39) and a lag time lag of 9; while the positive cc-ρ had a lag response of around 41 months and close to 0.3 in El Niño 3.4 region; the lag time is similar in El Niño 1 + 2 region. In the region El Niño 1 + 2, the spectral coherence was much more variable than in El Niño 3.4 region due to the oceanographic variability typical of coastal areas.

The spectral coherence functions of the indexes ONI and MEI (El Niño 3.4 region) were similar (Figs. 10 and 11b/c) to SST anomalies in El Niño 3.4 region in both lag response time and cc-ρ. The obtained spectral coherence of the cross-correlations functions would suggest a negative slope of the linear cross-correlation of ONI, MEI, SSTA, and lower SST in El Niño 3.4 region at the beginning of the cycles, as there is a least 12–24 months of low SS counts (less energy) before the sun start up increasing SS number, so the start of a new SS cycle. The negative cc-ρ of ONI, MEI, and SST would imply the occurrence of la Niña events of at least lower SST at the beginning of the ascending phase (or ending of descending phase) as there is lower heat content in the sea surface of El Niño 3.4 region due to lower TSI and SS counts. The highest cc-ρ would mean at least 14.4% of the index signals are due to SS activity.

The interdecadal indexes PDO and AMO correlated in a different manner in both ascending (Fig. 10a/d) and descending (Fig. 11a/d) phases. During the ascending phase, the PDO showed highly alternated slopes of the linear cross-correlation from positive to negative (Fig. 9a) in lags of 2–3 months around coefficients varying from −0.2 to 0.1, while the fluctuation of AMO smoothly fluctuated on larger lags from 9 to 24 months, with negative and positive slopes and similar coefficients (0.1 to > −0.2). However, during the descending phases, the pattern of fluctuation was somehow the contrary.

From the statistical point of view, the correlation coefficients from the cross-correlation method are a good measure of temporal similarity between time series. In other words, a high correlation coefficient does not imply a cause-effect relationship but rather means that the past values of the sunspots are good predictors of the values of the index series, as indicated by Hacker and Hatemi-J (2006). From the physical point of view, some authors have reported that SS cycle dynamics can produce 0.04–0.05C fluctuations of the sea surface temperature at a meter depth (Shaviv, 2008; Spencer, 2010). Zhou and Tung (2010) have found warming of 0.08C per each W m^{-2} variation of the TSI, and Shaviv (2008) suspects there is an unknown amplification phenomenon of the TSI impact on the sea surface, which could include solar wind and high sensitivity of the UV-region spectrum. Given the apparent, however discussed, climate system response to solar irradiance variability (see Dewitte et al., 2022), the results reported here imply that even though they are small in magnitude, but not negligible. The results also open the need for a continuous space-based solar irradiance monitoring as well as in situ measurement of the actual solar energy reaching the surface of the ocean. Improving the understanding of the physical causes of the solar irradiance, cosmogenic variability, UV irradiance variability and of the pathways by which the studied indexes respond to direct as well as indirect solar radiative forcing.

In this work all known statistical tools were used to avoid spurious correlation. The ENSO modelers should consider in some way the impacts of the SS cycles oscillations, especially during, their ascending or descending phases as well as their peaks and valleys, plus the possible amplifiers of solar energy. The needs and strives for a better modelling skills are amply recognized (Tao et al., 2020; Chen et al., 2022). For example, in the late northern hemisphere summer, there were some failed predictions for El Niño event 2018 (http://www.bom.gov.au/climate/enso/), the ONI was > +0.5C but the SOI did not match (http://www.cpc.ncep.noaa.gov/products/precip/CWlink/MJO/enso.shtml), as it should be in order to declare El Niño o La Niña (Bjerknes, 1969; Hu et al., 2020). One year later, Ludescher et al. (2019) predicted a strong El Niño by the end of 2020 with a probability of 4 out of 5 based on the algorithm so-called System Sample Entropy (Ludescher et al., 2014: Meng et al., 2020) that had rightly predicted three previous events. The announced El Niño 2020 did not only occur but there was the contrary event: La Niña with an ONI -1.3C and matched SOI by the end of the predicted year. Thus, generally, most current models are weak to provide consistent projections beyond 6 months, Yang et al. (2021) have

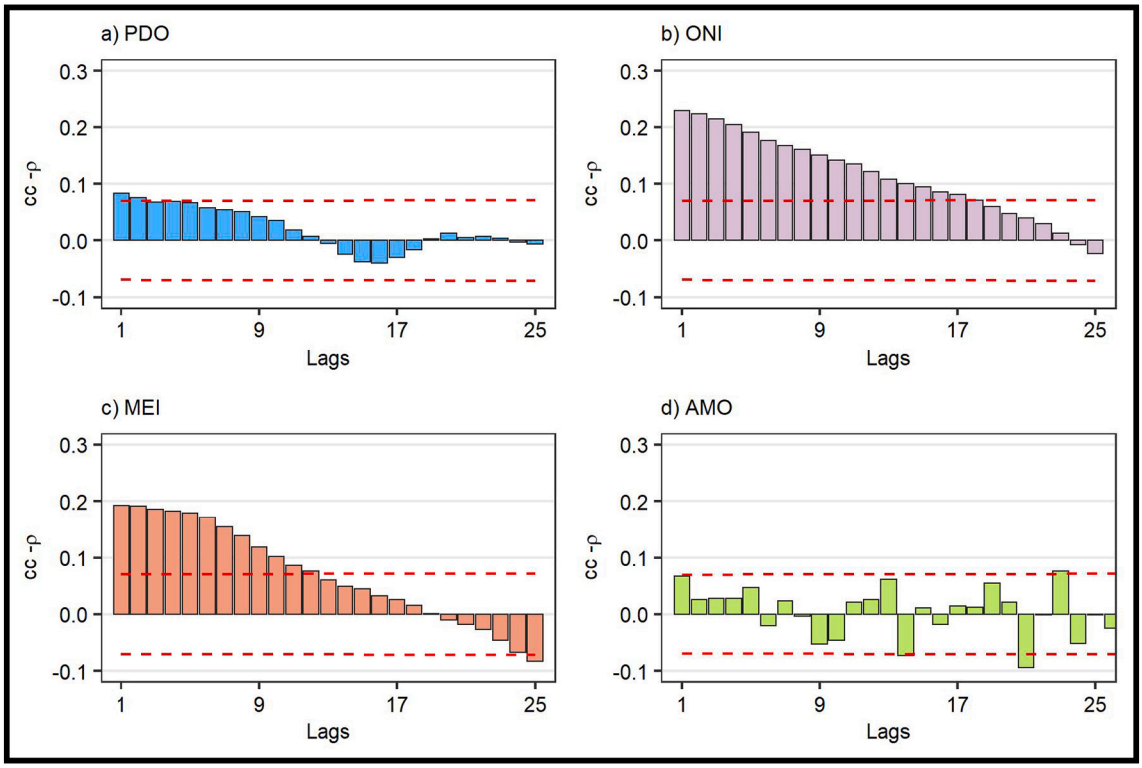

Fig. 11. Linear cross-correlation cc-ρ for all descending phases of SS cycles: a) PDO; b) ONI, c)MEI, and d) AMO.

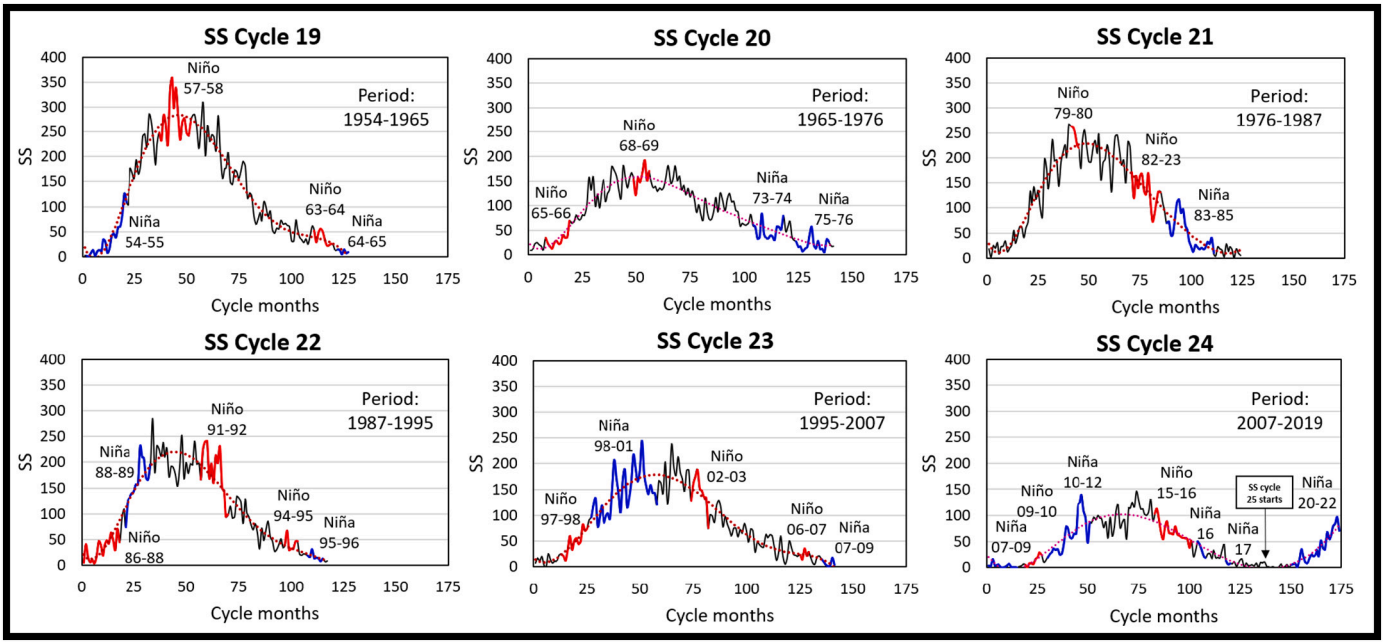

Fig. 12. Sunspots monthly counts curves per cycle. Red and blue lines represent El Niño and La Niña events. Note that Cycle 24 finished on December 2019 (National Weather Service, 2020). (For interpretation of the references to colour in this figure legend, the reader is referred to the web version of this article.)

recently discussed a series of variables to get El Niño, prediction models. La Niña 2020–2022 has extended for a third year in a row (see Johnson 2021; Jone, 2022). By last December La Niña CPC - Climate Weather Linkage: El Niño Southern Oscillation (noaa.gov), was declared extended up to March–April 2022 (Climate Driver Update (bom.gov.au)) with negative and positives SSTAs through the end of the first semester (El Niño Southern Oscillation (ENSO) region sea surface temperature forecasts - Met Office). It was also projected with 60% chances, that transition to ENSO-neutral would start during Abril-June [(CPC - Climate Weather Linkage: El Niño Southern Oscillation (noaa.gov), January 10, 2022)]. Now, at July 2022, La Niña is predicted to go all along 2022, and even more, some voices are saying till 2023.

The results presented here are in harmony to La Niña 2020–2022, because cycle 25 have just started after a long period of very low sunspots counts and months without them; also the PDO Indexes have been strongly and continuously negative; during 1999–2022, −0.65C; 2020–2021, −1.05C; and last semester 2022, −2.08C; see, https://www.ncdc.noaa.gov/teleconnections/pdo/. This cold PDO phase started around 2000 and will last till 2025–2030, and it converges the fact, that since 2018 the SS monthly counts were <10 with many weeks without any SS (http://www.sws.bom.gov.au/Solar/1/6). These low SS counts continued through the end of 2019. The input of solar heat has been at its lowest values since the 1950s.

4. Conclusions

Over the studied period 1954–2019, sunspot numbers decreased from a monthly maximum between 225 (SS 21) to a minimum around 20–25 (SS 24). The SS 24 had 913 days without SS counts until December 2019 (Burud et al., 2021), being this cycle the weakest since 1755; and the SS 25 will probably be weaker than or like SS 24 (Ineson et al., 2014; Chowdhury et al., 2021; NASA, 2021a, 2021b). Thus, the Earth has been receiving slightly decreasing solar energy over this almost 7-decade period.

In general, the influence of the whole series of Schwabe cycles (19–24) and the studied indexes had statistically significant but poor o limited cross-correlation coefficients (0.063–0.100), with a possible influence of 0.4–1.0%, with lag times from 3 to 46 months. Recently, Le Mouël et al. (2019) have ratified the strong link between climate and solar activity arguing that the mechanisms must be complex and in the realm of non-linearity with UV radiation variation, solar wind, etc. as possible variables. The Schwabe cycles fluctuations could have an important impact on the global climate (Ermolli et al., 2013). Nonetheless, Gil et al. (2014) have found no significant statistical relation between sunspots and global temperature.

On the ocean surface the influence of sunspots could chiefly be due to UV energy fluctuation (Ineson et al., 2014) as this radiation penetrates down to 75–100 m depth in the water column (Smyth, 2011). van Loon et al. (2007) suggested that even though SS cycles produce weak changes on the Total Solar Irradiation (TSI) of about 0.07% (Gray et al., 2010), these can still produce decadal and millennial impacts on global thermohaline circulation (Bond et al., 2001; Gray et al., 2016).

Thus, 1) short term differences between individual cycles, like the 19 and 24 for example with different maxima of SS counts or time length; 2) the medium time scale variation behaviour of inner solar processes during several cycles (Maunder Minimum); 3) the variability of the UV radiation; and 4) longer processes as the Gleissberg cycle with a period of roughly 80 to 90 years cycle could be slightly affecting the impacts of SS cycles over the studied indexes on decadal periods.

Individual SS cycles (19–24). The SST and SSTAs showed low cross-correlation against every individual SS cycle in El Niño 3.4 and El Niño 1 + 2 regions with coefficients from 0.100 to 0.200 with lag times from few months to 2–3 years. In El Niño 1 + 2 region, the sunspot activity could influence the SST and SSTA, but the relatively low coefficients may well reflect high seasonal and inter-annual variability in coastal oceanographic conditions; while in El Niño 3.4 region, the influence of regional oceanographic and meteorological conditions could be the driving factors.

The ONI Index showed to be poorly cross-correlated with cc-ρ values <0.100, only twice approached to −0.200. On the other hand, the MEI registered around ±0.200 through all cycles and predominant lag times within 12 months. The SOI showed cross-correlations with SS cycles (19–21, and) averaging a coefficient of 0.200 with lags times range of 9–34 months. The SOI temporal behaviour has also been associated with SS and it could enhance or affect the oceanographic Indexes of the equatorial Pacific (Higginson et al., 2004).

The PDO would have been affected up to 8% by the individual Schwabe cycles, and it is in synchrony with the periods of cold and warm

phases. There is a direct and consistent relationship between PDO with ONI or MEI has been reported extensively (e.g., Jia and Ge, 2017; Karmouche, 2020). Equally, AMO could have been associated also up to 8% to individual SS cycles, with a spectral coherence within the lag time of 1–3 years. The PDO and AMO cross-correlations seemed to alternate. Li et al. (2016) said these indexes are in quasi opposite phases (see also http://appinsys.com/globalwarming/amo.htm). It is noteworthy that the slopes of the PDO and AMO linear cross-correlations are negative and positive respectively for cycles 21 and 22 (warm PDO), but in concordance in cycles 19, 20, 23, and 24 (cold PDO).

In El Niño 3.4 region, during the ascending and declining phases of the SS cycles cross correlation with SSTs had coefficients up to +0.288 and − 0.233, respectively, which represents an influence of up to 8.2% on the SSTs values. In El Niño 1 + 2 region cross correlations were negligible in both ascending and descending phase. It seems that short-time expressions of SS cycles, either at the beginning of their ascending or descending phases, have a positive but variable effect on the SSTs depending on each cycle. Thus, the warm events El Niño of 1957–1958 (SS 19), 1965–1966 (SS 20), 1981–1982 (SS 21), 1987–1988 and 1991–1992 (SS 22), 1997–1998 (SS 23), 2015–2016 (SS 24) have each one its own peculiarity. On the other hand, the cold events of La Niña tend to occur after an El Niño at the middle of the ascending phases (1988–1989, 1999–2001, 2010–2012) or when approaching, during and leaving the minimum of the cycles (1954–1956, 1973–1974, 1975–1976; 1995–1996, 2007–2009, 2017–2018, 2020–2022). The last three La Niña events are associated with extremely low and lengthy periods of absence of sunspots (see Schrijver et al., 2011). On the other hand, the so-called equatorial Pacific neutral conditions in El Niño 3.4 region (https://iridl.ldeo.columbia.edu/maproom/ENSO/ENSO_Info.html), seems to span a longer period after La Niña, and vice versa after El Niño.

The ENSO Indexes ONI and MEI also showed stronger cross-correlations to the ascending phase of the Schwabe cycles, with a lag time of 1–15 months, probably affecting up to 20.1% during cycle SS 21 (big El Niño and La Niña), but during the declining phase the ONI was affected by 4.9%. Besides, it was found that warm events tend to occur in the ascending phases (as TSI increases) or at the top of the cycles. These warm events have a delay time of 24 months (see Huo and Xiao, 2016), whilst cold events are mostly associated with a descending phase but with a quicker response time of 0–12 months.

The MEI index could have been influenced from 7.3% up to 23%. The MEI correlated in all ascending and descending phases of SS cycles. The SOI had similar cross-correlation coherence to those oceanographic indexes during ascending and descending phases. These results would provide evidence on how SS affects the studied Indexes during the ascending/descending phases of their cycles. In some cycles, the impact will be stronger and in other weaker depending on intensity and behaviour in time of the cycle.

The PDO registered the highest linear cross-correlation coefficients up to 0.417 and − 0.491 during ascending phases, except the SS cycle 21. During descending phase, the highest cc-ρ was −0.348 with lag times were between 1 and 37 months, in all cycles. Meanwhile, the AMO index appeared to be systematically influenced through all cycles during both ascending and descending phases with an influence of SS up to 30.2% and 10% respectively. During the studied period fluctuations of TSI were up twice this value in some cases like in 1984 and 1989. These changes can be reflected by PDO and AMO Indexes. However, the Intergovernmental Panel on Climate Change (IPPC, 2001) considers this fact too small to drive climate changes (Wang et al., 2017a, 2017b).

Further exercises, using the compiled data for all the ascending and descending phases of all 6 cycles, suggested that SST and SSTA in both regions showed to have inverse and direct linear relationship with SS at lags times around 9 and direct 50 months, respectively. The spectral coherence resemblance a sine function, which is much more defined during ascending phases. The coefficients were stronger during ascending than descending phase. The variations from 8 to 15% of these indexes could be explained by the fluctuations of Schwabe cycles.

The indexes used to define cold or warm events in the Central equatorial Pacific Ocean, SOI, ONI, and MEI responded to the ascending SS phase in a comparable manner to SST and SSTA in El Niño 3.4 region, with a minimum cc-ρ of −0.33 and − 0.38 and maxima of 0.39 and 0.25 in the same order, and similar lag times of around 8 and 40 months. From this data, we could suggest that at the beginning of the cycles there is inverse linear regression, but a direct relationship from 8 to 9 months to over 40 months, then again inverse linear relationship for about 12 months. During the descending phase, both indexes showed a direct linear relationship for nearly 2 years. The variations of ONI and MEI could be justified 6–15% and 4% by the variation of SS during the ascending and descending phases of the cycles, respectively. The inter-annual cycles PDO and AMO seemed not to be strongly affected by the ascending and descending phases, probably because these indexes have fluctuations in the order of 25 years (>2.5 SS cycles). During cold PDO, La Niña events are more frequent and stronger than El Niño, and vice versa during warm PDO. In here, the SS cycles 19–20, 23–24, and 21–22 were registered during cold, warm, and cold PDOs.

Finally, did Schwabe cycles 19–24 influence the ENSO events, PDO, and AMO indexes in the Pacific and Atlantic Oceans? Yes, it has been found a wide range correlation coefficient from 0.100 to about 0.500 statistically significant ($p < 0.05$) with lag times from few months to over 2 years between the Schwabe cycles and the ocean indices chosen here. These results could be a potential source to improve predictive skills for the understanding of ENSO, PDO and AMO interannual and decadal fluctuations. Better predictive models are imperative given that El Niño or La Niña has vast impacts on lives, property, and economic activity around the globe, especially when dramatic peaks of El Niño occur. The new cycle 25 has started and could have a major oceanic swing follow suit, and the next El Niño would be in around 2023–2024 according to historical events and results presented here.

Data availability

All data are publicly available on the Web (see Material and Methods).

Author contributions

FIO-G conceptualized, constructed the hypotheses, designed the material and methods, and drafted the paper in all its stages and oversaw the project. MEE-C retrieved and treated all data/information organized results, designed, and constructed graphs. HR-L statistical work and methods. All authors participated in every step of the research.

Declaration of Competing Interest

The authors declare that they have no known competing financial interests or personal relationships that could have appeared to influence the work reported in this paper.

Data availability

Data available in supplementary material.

Acknowledgements

Authors are grateful to ESPOL authorities whose supported research allotting time and financial resources to present this paper in the “4TH INTERNATIONAL SYMPOSIUM: THE CLIMATE CHANGE EFFECTS ON THE WORLD OCEANS” held in Washington DC, 4-8 June 2018, also The National Chamber of Fisheries of Ecuador support is acknowledged. This manuscript was released as a pre-print at Ocean Sci. Discuss., https://doi.org/10.5194/os-2018-125, 2018. (Ormaza-González, F. I. and Espinoza-Celi, M). Work on the language, reviewing and editing from

Professor Peter Statham (Southampton University, UK) and Professor John Huthnance (NOC-UK) is appreciated. Dafne Vera-Mosquera and anonymous scientists also contributed to improve initial manuscript.

In the Memory: Eloy Ortega (Ecuadorian Astronomer)

Appendix A. Supplementary data

Supplementary data to this article can be found online at https://doi.org/10.1016/j.gloplacha.2022.103928.

References

Albert, J., Krishnan, A., Bhaskaran, P.K., et al., 2022. Role and influence of key atmospheric parameters in large-scale environmental flow associated with tropical cyclogenesis and ENSO in the North Indian Ocean basin. Clim. Dyn. 58, 17–34. https://doi.org/10.1007/s00382-021-05885-8.

Allan, R.J., Ansell, T., 2006. A new globally complete monthly historical gridded mean sea level pressure dataset (HadSLP2): 1850-2004. J. Clim. 19, 5816–5842.

Allan, R.J., Nicholls, N., Jones, P.D., Butterworth, I.J., 1991. A further extension of the Tahiti-Darwin SOI, early SOI results and Darwin pressure. J. Clim. 4, 743–749.

Ashok, K., Behera, S.K., Rao, S.A., Weng, H., Yamagata, T., 2007. El Niño Modoki and its possible teleconnection. J. Geophys. Res. 112, C11007 https://doi.org/10.1029/2006JC003798.

Asma, Zaffar, Abbas, S., Ansari, M.R., 2019. An analysis of heavy tail and long-range correlation of sunspot and el nino-southern oscillation (ENSO) cycles. Sol. Syst. Res. 53, 399–409. https://doi.org/10.1134/S0038094619050010.

Barnston, A., 2015. Why are There So Many ENSO Indexes, Instead of Just One? https://www.climate.gov/news-features/blogs/enso/why-are-there-so-many-enso-Indexes-instead-just-one (last access: 15 March 2018).

Bhowmik, P., Nandy, D., 2018. Prediction of the strength and timing of sunspot cycle 25 reveal decadal-scale space environmental conditions. Nat. Commun. 9, 5209. https://doi.org/10.1038/s41467-018-07690-0.

Bjerknes, J., 1969. Atmospheric teleconnections from the equatorial Pacific. Mon. Weather Rev. 97, 163–172. https://doi.org/10.1175/1520-0493(1969)097<0163:ATFTEP>2.3.CO;2.

Bond, G.G., Kromer, B., Beer, J., Muscheler, R., Evans, M., Showers, W., Hoffmann, S., Lotti-Bond, R., Hajdas, I., Bonani, G., 2001. Persistent solar influence on North Atlantic climate during the holocene. Science 294, 2130–2136.

Brown, J.L., 1957. On a cross-correlation property for stationary random processes. IRE Trans. Inf. Theory 3 (1), 28–31. https://doi.org/10.1109/TIT.1957.1057390.

Burud, D.S., Jain, R., Awasthi, A.K., Chaudhari, S., Tripathy, S.C., Gopalswamy, N., Chamadia, P., Kaushik, S.C., Vhatkar, R., 2021. Spotless days and geomagnetic index as the predictors of solar cycle 25. RAA 21 (9). https://doi.org/10.1088/1674-4527/21/9/215.

Busalacchi, A.J., Takeuchi, K., O'Brien, J.J., 1983. Interannual variability of the equatorial Pacific-revisited. J. Geophys. Res. 88, 7551–7562.

Cheke, R.A., Young, S., Wang, X., Tratalos, J.A., Tang, S., Cressman, K., 2021. Evidence for a causal relationship between the solar cycle and locust abundance. Agronomy 11, 69. https://doi.org/10.3390/agronomy11010069.

Chen, X., Tung, K.K., 2014. Varying planetary heat sink led to global-warming slowdown and acceleration. Science 345, 897–903. https://doi.org/10.1126/science.1254937.

Chen, N., Fang, X., Yu, J.Y., 2022. A multiscale model for El Niño complexity. npj Clim Atmos Sci 5, 16. https://doi.org/10.1038/s41612-022-00241-x.

Chowdhury, P., Jain, R., Ray, P.C., et al., 2021. Prediction of amplitude and timing of solar cycle 25. Sol. Phys. 296 (69), 2021. https://doi.org/10.1007/s11207-021-01791-8.

Clette, F., Svalgaard, L., Vaquero, J.M., Cliver, E.W., 2014. Revisiting the sunspot number. Space Sci. Rev. 186, 35–103. https://doi.org/10.1007/s11214-014-0074-2.

Clutz, R., 2017. Global Ocean Cooling in September. https://rclutz.wordpress.com/2017/10/26/global-ocean-cooling-in-september/ (last access: 30 October 2017).

Condron, A., DeConto, R., Bradley, R.S., Juanes, F., 2005. Multidecadal North Atlantic climate variability and its effect on North American salmon abundance. J. Geophys. Res. Lett. https://doi.org/10.1029/2005GL024239, 32L23703.

Dewitte, S., Cornelis, J., Meftah, M., 2022. Centennial total solar irradiance variation. Remote Sens. 14 (5), 1072. https://doi.org/10.3390/rs14051072.

Dicke, R.H., 1978. Is there a chronometer hidden deep in the Sun? Nature 276, 676–680.

Ding, A., Hofmann, A., Li, Y.L., 2022. 2470-million-year-old banded iron formation reveals a climatic oscillation consistent with the Gleissberg solar cycle. Commun. Earth Environ. 3, 45. https://doi.org/10.1038/s43247-022-00378-w.

d'Orgeville, M., Peltier, W.R., 2007. On the pacific decadal oscillation and the atlantic multidecadal oscillation: might they be related? Geophys. Res. Lett. 34, L23705. https://doi.org/10.1029/2007GL031584.

Eddy, J.A., 1976. The maunder minimum. Science 192 (4245), 1189–1202. https://doi.org/10.1126/science.192.4245.1189.

Enfield, D.B., Mestas-Nuñez, A.M., Trimble, P.J., 2001. The Atlantic multidecadal oscillation and its relation to rainfall and river flows in the continental US. J. Geophys. Res. Lett. 28, 2077–2080. https://doi.org/10.1029/2000GL012745.

Ermolli, I., Matthes, K., Dudok de Wit, T., Krivova, N.A., Tourpali, K., Weber, M., Unruh, Y.C., Gray, L., Langematz, U., Pilewskie, P., Rozanov, E., Schmutz, W., Shapiro, A., Solanki, S.K., Woods, T.N., 2013. Recent variability of the solar spectral irradiance and its impact on climate modelling. Atmos. Chem. Phys. 13, 3945–3977. https://doi.org/10.5194/acp-13-3945-2013.

Fang, X., Zheng, X., Zhang, X., 2020. Correspondence between the large volcanic eruptions and ENSO events over AD 1525–2000. J. Geogr. Sci. 30, 103–118. https://doi.org/10.1007/s11442-020-1717-8.

Fasullo, J., Nerem, R., 2016. Interannual variability in global mean sea level estimated from the CESM large and last millennium ensembles. Water 8, 491. https://doi.org/10.3390/w8110491.

Fröhlich, C., 2013. Solar constant and total solar irradiance variations. In: Richter, C., Lincot, D., Gueymard, C.A. (Eds.), Solar energy. Springer, New York, NY.

Galilei, Galileo, 1613. Letters on Sunspots. British Library. https://www.bl.uk/collection-items/galileos-sunspot-letters.

Gil, L.A., Yaya, O.S., Shittu, O.I., 2014. Global temperatures and sunspot numbers. Are they related? Physica A. 396, 42–50.

Gill, A.E., 1982. Atmosphere–Ocean Dynamics, International Geophysics Series. Academic Press edited by: Donn, W. L., 30, 662 pp., eBook ISBN: 9780080570525, Paperback ISBN: 9780122835223.

Glantz, M.H., 2001. Once Burned, Twice Shy? Lessons Learned from the 1997-1998 El Niño. The Unite Nations University, 294 pp.

Granger, C.W.J., 1986. Developments in the study of cointegrated economic variables. Oxf. Bull. Econ. Stat. 48 (3), 213–228. https://doi.org/10.1111/J.1468-0084.1986.MP48003002.X.

Gray, L.J., Beer, J., Geller, M., Haigh, J.D., Lockwood, M., Matthes, K., Cubasch, U., Fleitmann, D., Harrison, G., Hood, L., Luterbacher, J., Meehl, G.A., Shindell, D., van Geel, B., White, W., 2010. Solar influences on climate. Rev. Geophys. 48, RG4001 https://doi.org/10.1029/2009RG000282.

Gray, L.J., Woollings, T.J., Andrews, M., Knight, J., 2016. Eleven-year solar cycle signal in the NAO and Atlantic/European blocking. Q. J. Roy. Meteor. Soc. 142, 1890–1903. https://doi.org/10.1002/qj.2782.

Hacker, R.S., Hatemi-J, A., 2006. Tests for causality between integrated variables using asymptotic and bootstrap distributions: theory and application. Appl. Econ. 38 (13), 1489–1500. https://doi.org/10.1080/00036840500405763.

Hady, Ahmed A., 2013. Deep solar minimum and global climate changes. J. Adv. Res. 4 (3), 209–214. https://doi.org/10.1016/j.jare.2012.11.001 (ISSN: 2090–1232).

Hansen, J., Kharecha, P., Sato, M., Masson-Delmotte, V., Ackerman, F., et al., 2013. Assessing "Dangerous Climate Change": Required reduction of carbon emissions to protect young people, future generations and nature. PLoS One 8 (12), e81648. https://doi.org/10.1371/journal.pone.0081648.

Hassan, D., Iqbal, A., Hassan, S.A., Abbas, S., Ansari, M.R.K., 2016. Sunspots and ENSO relationship using Markov method. J. Atmos. Sol. Terr. Phys. 137, 53–57. https://doi.org/10.1016/j.jastp.2015.11.017.

Hathaway, D.H., 2015. The solar cycle. Living Rev. Sol. Phys. 12, 4. https://doi.org/10.1007/lrsp-2015-4.

Henley, B.J., Gergis, J., Karoly, D.J., Power, S., Kennedy, J., Folland, C.K., 2015. A tripole index for the interdecadal pacific oscillation. Clim. Dyn. 45, 3077. https://doi.org/10.1007/s00382-015-2525-1.

Higginson, M.J., Altabet, M.A., Wincze, L., Herbert, T.D., Murray, D.W., 2004. A solar (irradiance) trigger for millennial-scale abrupt changes in the southwest monsoon? Paleoceanography 19, PA3015. https://doi.org/10.1029/2004PA001031.

Horning, N., Russell, C., Goetz, S., 2003. Energy from the Sun to Earth's surface. In: Chapter 2: Earth's Radiation Balance and the Global Greenhouse. https://people.ucsc.edu/~mdmccar/migrated/ocea80b/public/lectures/lect_notes_1/03_Energy_Balance_MDM_11F.pdf (last access: 25 April 2018).

Hu, Z.-Z., McPhaden, M.J., Kumar, A., Yu, J.-Y., Johnson, N.C., 2020. Uncoupled El Niño warming. Geophys. Res. Lett. 47 https://doi.org/10.1029/2020GL087621 e2020GL087621.

Huang, B., Banzon, V.F., Freeman, E., Lawrimore, J., Liu, W., Peterson, T.C., Smith, T.M., Thorne, P.W., Woodruff, S.D., Zhang, H.M., 2014. Extended reconstructed sea surface temperature version 4 (ERSST.v4): part I. Upgrades and intercomparisons. J. Clim. 28, 911–930. https://doi.org/10.1175/JCLI-D-14-00006.

Huang, B., Thorne, P.W., Banzon, V.F., Boyer, T., Chepurin, G., Lawrimore, J.H., Menne, M.J., Smith, T.M., Vose, R.S., Zhang, H.M., 2017. Extended reconstructed sea surface temperature, Version 5 (ERSSTv5): Upgrades, validations, and intercomparisons. J. Clim. 30, 8179–8205. https://doi.org/10.1175/JCLI-D-16-0836.1.

Huo, W.J., Xiao, Z.N., 2016. The impact of solar activity on the 2015/16 El Niño event. Atmos. Oceanic Sci. Lett. https://doi.org/10.1080/16742834.2016.1231567.

Ineson, S., Maycock, A.C., Gray, L.J., Scaife, A.A., Dunstone, N.J., Harder, J.W., Knight, J.R., Lockwood, M., Manners, J.C., Wood, R.A., 2015. Regional climate impacts of a possible future grand solar minimum. Nat. Commun. 6, 7535. https://doi.org/10.1038/ncomms8535.

Jenkins, G.M., Watts, D.G., 1968. Spectral Analysis and Its Applications. Holden-Day, San Francisco.

Jia, X., Ge, J., 2017. Modulation of the PDO to the relationship between moderate ENSO events and the winter climate over North America. Int. J. Climatol. 37, 4275–4287. https://doi.org/10.1002/joc.5083.

Jone, N., 2022. Rare 'triple' La Niña climate event looks likely — what does the future hold? Nat. News. https://doi.org/10.1038/d41586-022-01668-1, 22 June.

Jones, P., 2017. The reliability of global and hemispheric surface temperature records. Adv. Atmos. Sci. 33 (3), 269–282. https://doi.org/10.1007/s00376-015-5194-4.

Karmouche, S., 2020. Understanding Dependency Structures in Major Modes of Climate Variability with Causal Discovery. MSc Thesis. Bremen University. https://www.uni-bremen.de/en/university.html.

Kerr, R.A., 2000. A North Atlantic climate pacemaker for the centuries. Science 288, 1984–1985.

Komitov, B., Kaftan, V., 2013. The sunspot cycle no. 24 in relation to long term solar activity variation. J. Adv. Res. 4 (3), 279–282. https://doi.org/10.1016/j.jare.2013.02.001.

Können, G.P., Jones, P.D., Kaltofen, M.H., Allan, R.J., 1998. Pre-1866 extensions of the Southern Oscillation Index using early Indonesian and Tahitian meteorological readings. J. Clim. 11, 2325–2339.
Kopp, G., Lean, J.L., 2011. A new, lower value of total solar irradiance: Evidence and climate significance. J. Geophys. Res. Lett. https://doi.org/10.1029/2010GL045777, 38L01706.
Kristoufek, L., 2017. Has global warming modified the relationship between sun spot numbers and global temperatures? Physica A. 468, 351–358. https://doi.org/10.1016/j.physa.2016.10.089.
Lander, M.A., 1994. An exploratory analysis of the relationship between tropical storm formation in the Western North Pacific and ENSO. Mon. Weather Rev. 4 (3), 57–71. http://marefateadyan.nashriyat.ir/node/150.
Laurenz, L., Lüdecke, H.-J., Lüning, S., 2019. Influence of solar activity on European rainfall. J. Atmos. Solar-Terres. Phys. 185, 29–42. https://doi.org/10.1016/j.jastp.2019.01.012.
Le Mouël, J.-L., Lopes, F., Courtillot, V., 2019. A solar signature in many climate indices. J. Geophys. Res. Atmos. 124, 2600–2619. https://doi.org/10.1029/2018JD028939.
Leamon, R.J., McIntosh, S.W., Chapman, S.C., et al., 2020. Timing terminators: forecasting sunspot cycle 25 onset. Sol. Phys. 295, 36. https://doi.org/10.1007/s11207-020-1595-3.
Leamon, R.J., McIntosh, S.W., Marsh, D.R., 2021. Termination of solar cycles and correlated tropospheric variability. Earth Space Sci. 8 https://doi.org/10.1029/2020EA001223 e2020EA001223.
Lean, J.L., Beer, J., Bradley, R.S., 1995. Reconstruction of solar irradiance since 1610: Implications for climate change. Geophys. Res. Lett. 22, 3195–3198.
Li, A.K., Paek, H., Yu, J.-Y., 2016. The changing influences of the AMO and PDO on the decadal variation of the Santa Ana winds. Environ. Res. Lett. 11, 064019. https://doi.org/10.1088/1748-9326/11/6/064019.
Lindsey, R., 2009. Climate and earth's energy budget. In: NASA Earth Observatory. https://earthobservatory.nasa.gov/Features/EnergyBalance/ (last access: 25 April 2018).
Lindsey, R., 2013. In Watching for El Niño and La Niña, NOAA Adapts to Global Warming. https://www.climate.gov/news-features/understanding-climate/watching-el-ni%C3%B1o-and-la-ni%C3%B1a-noaa-adapts-global-warming (last access: 25 April 2018).
Liu, F., Chai, J., Huang, G., Liu, J., Chen, Z., 2015. Modulation of decadal ENSO-like variation by effective solar radiation. Dyn. Atmos. Oceans 72, 52–61. ISSN: 0377–0265.
Llanes-Cárdenas, O., Norzagaray-Campos, M., Gaxiola, A., et al., 2020. Regional precipitation teleconnected with PDO-AMO-ENSO in northern Mexico. Theor. Appl. Climatol. 140, 667–681. https://doi.org/10.1007/s00704-019-03003-7.
Lockwood, M., 2010. Solar change and climate: an update in the light of the current exceptional solar minimum. P. Roy. Soc. A-Math Phy. 466, 303–329.
Lockwood, M., 2013. Reconstruction and prediction of variations in the open solar magnetic flux and interplanetary conditions. Living Rev. Sol. Phys. 10, 4.
Lübbecke, J.F., Rudloff, D., Stramma, L., 2019. Stand-alone eastern Pacific Coastal Warming events. Geophys. Res. Lett. 46, 12360–12367. https://doi.org/10.1029/2019GL084479.
Ludescher, J., Gozolchiani, A., Bogachev, M.I., et al., 2014. Very early warning of next El Niño. Proc. Natl. Acad. Sci. U. S. A. 111 (6), 2064–2066. https://doi.org/10.1073/pnas.1323058111.
Ludescher, J., Bunde, Armin, Havlin, Shlomo, Schellnhuber, Hans Joachim, 2019. Very early warning signal for El Niño in 2020 with a 4 in 5 likelihood. Pre-print. arXiv: 1910.14642.
Maleski, J.J., Martinez, C.J., 2018. Coupled impacts of ENSO AMO and PDO on temperature and precipitation in the Alabama–Coosa–Tallapoosa and Apalachicola–Chattahoochee–Flint river basins. Int. J. Climatol. 38, e717–e728. https://doi.org/10.1002/joc.5401.
Mantua, N.J., Hare, S.R., 2002. The Pacific decadal oscillation. J. Oceanogr. 58, 35–44.
Mantua, N.J., Hare, S.R., Zhang, Y., Wallace, J.M., Francis, R.C., 1997. A Pacific interdecadal climate oscillation with impacts on salmon production. B. Am. Meteorol. Soc. 78, 1069–1079.
McCarthy, G., Haigh, I., Hirschi, JM., et al., 2015. Ocean impact on decadal Atlantic climate variability revealed by sea-level observations. Nature 521, 508–510. https://doi.org/10.1038/nature14491.
McKinley, G.A., Takahashi, T., Buitenhuis, E., Chai, F., Christian, J.R., Doney, S.C., Jiang, M.-S., Lindsay, K., Moore, J.K., Le Quéré, C., Lima, I., Murtugudde, R., Shi, L., Wetzel, P., 2006. North Pacific carbon cycle response to climate variability on seasonal to decadal timescales. J. Geophys. Res. 111 https://doi.org/10.1029/2005JC003173. C07S06.
Meehl, G.A., Arblaster, J.M., Matthes, K., Sassi, F., van Loon, H., 2009. Amplifying the Pacific climate system response to a small 11-year solar cycle forcing. Science 325, 1114–1118.
Meng, J., Fan, Jingfang, Ludescher, Josef, Agarwal, Ankit, Chen, Xiaosong, Bunde, Armin, Kurths, Jürgen, Schellnhuber, Hans Joachim, Jan 2020. Complexity-based approach for El Niño magnitude forecasting before the spring predictability barrier. Proc. Natl. Acad. Sci. 117 (1), 177–183. https://doi.org/10.1073/pnas.1917007117.
Miyahara, H., Tokanai, F., Moriya, T., et al., 2021. Gradual onset of the Maunder Minimum revealed by high-precision carbon-14 analyses. Sci. Rep. 11, 5482. https://doi.org/10.1038/s41598-021-84830-5.
Montecino, V., Lange, C.B., 2009. The Humboldt Current System: Ecosystem components and processes, fisheries, and sediment studies. Prog. Oceanogr. 83, 65–79.
Mörner, N.-A., 2015. The approaching new grand solar minimum and little ice age climate conditions. Nat. Sci. 7, 510–518. https://doi.org/10.4236/ns.2015.711052.
NASA, 2021a. Solar Cycle 25 is Here. NASA, NOAA Scientists Explain What That Means. https://www.nasa.gov/press-release/solar-cycle-25-2020. Latest access 10 April 2021.
NASA, 2021b. Solar Cycle 25 Preliminary Forecast | NOAA / NWS Space Weather Prediction Center. Latest access 11 May 2021.
National Weather Service, 2020. Hello Solar Cycle 25. Retrieved 9 December 2021.
Newman, M., Compo, G.P., Alexander, M.A., 2003. ENSO-forced variability of the Pacific decadal oscillation. J. Clim. 16, 3853–3857. https://doi.org/10.1175/1520-0442(2003)016<3853:EVOTPD>2.0.CO;2.
NOAA, 2016. El Niño and La Niña Alert System. https://www.climate.gov/news-features/understanding-climate.
Ormaza-González, F.I., 2016. Eventos oceanográficos de alta y baja frecuencia en El Océano Pacífico Ecuatorial Este. Revista Internacional de Investigación y Docencia (RIID) ISSN (Online): 2445–1711.
Ormaza-González, F.I., October 15, 2021. Onda Kelvin fría se aproxima a El Niño 1+2 region. La Niña Evoluciona en El Niño 3.4 region. Cámara Nacional de Pesquería. Análisis De Pesquerías Y Condiciones Oceanográficas. Latest Access January 2022.
Ormaza-González, F.I., Cedeño, J., 2017. Coastal El Niño 2017 or simply: the carnival coastal warming event? MOJ Ecol. Environ. Sci. 2 https://doi.org/10.15406/mojes.2017.02.00054, 00054.
Ormaza-González, F.I., Sánchez, E., 1983. Cálculo computacional del flujo de energía solar cobre el océano y su aplicación a la zona ecuatorial. Rev. Cienc. Mar Limnol. (INP-Ecuador) 2 (1), 27–54. ISSN 1390–5767.
Ormaza-González, F.I., Mora, A., Bermúdez, R.M., Hurtado, M.A., Peralta, M.R., Jurado, V.M., 2016a. Can small pelagic fish landings be used as predictors to high frequency oceanographic fluctuations in the 1-2 El Niño region? Adv. Geosci. 42, 61–72. https://doi.org/10.5194/adgeo-42-61-2016.
Ormaza-González, F.I., Mora, A., Bermúdez, R.M., 2016b. Relationships between tuna catch and variable frequency oceanographic conditions. Adv. Geosci. 42, 83–90. https://doi.org/10.5194/adgeo-42-83-2016.
Peek, K., 2018. Sunspot surprise. Sci. Am. 319, 2, 84. https://doi.org/10.1038/scientificamerican0818-84.
Peristykh, A.N., Damon, P.E., 2003. Persistence of the Gleissberg 88-year solar cycle over the last ~12,000 years: Evidence from cosmogenic isotopes. J. Geophys. Res. 108 (A1), 1003. https://doi.org/10.1029/2002JA009390.
Pishkalo, M.I., 2021. Prediction of solar cycle 25: maximum in the N- and S-hemispheres. Kinemat. Phys. Celest. Bodies 37, 27–32. https://doi.org/10.3103/S0884591321010050.
Podobnik, B., Stanley, H.E., 2008. Detrended cross-correlation analysis: a new method for analyzing two non-stationary time series. Phys. Rev. Lett. 100 (8) https://doi.org/10.1103/PhysRevLett.100.084102.
Porch, W.M., Olsen, S.C., Chylek, P., Dubey, M.K., Henderson, B.G., Clodius, W., 2006. Satellite and surface observations of Nauru Island clouds: differences between El Nino and La Nina periods. Geophys. Res. Lett. 33, L13804 https://doi.org/10.1029/2006GL026339.
Qian, Z., 2017. Evidence for the effect of sunspot activity on El Niño/Southern Oscillation. New Astron. 52, 1–7. https://doi.org/10.1016/j.newast.2016.09.004.
Ramírez, I.J., Briones, 2017. Understanding El Niño Costero of 2017: The definition problem and challenges of climate forecasting and disaster responses. F. Int J Disaster Risk Sci 8, 489. https://doi.org/10.1007/s13753-017-0151-8.
Rasmussen, E.M., Carpenter, T.H., 1982. Variations in tropical sea surface temperature and surface wind fields associated with the Southern Oscillation/El Niño. Mon. Weather Rev. 110, 354–384.
Raspopov, O.M., Dergachev, V.A., Esper, J., Kozyreva, O.V., Frank, D., Ogurtsov, M., Kolström, T., Shao, X., 2008. The influence of the de Vries (~200-year) solar cycle on climate variations: results from the Central Asian Mountains and their global link. Palaeogeogr. Palaeoclimatol. Palaeoecol. 259 (1), 6–16. https://doi.org/10.1016/j.palaeo.2006.12.017.
Reid, G.C., 2000. Solar variability and the Earth's climate: Introduction and overview. Space Sci. Rev. 94, 1–11. https://doi.org/10.1175/JCLI-D-11-00571.1.
Scafetta, N., 2014. Global temperatures and sun spot numbers. Are they related? Yes, but non-linearly. A reply to Gil-Alana et al. (2014). Physica A. 413, 329–342. https://doi.org/10.1016/j.physa.2014.06.047.
Scafetta, N., Willson, R.C., Lee, J.N., Wu, D.L., 2019. Modelling quiet solar luminosity variability from TSI satellite measurements and proxy models during 1980–2018. Remote Sens. 11 (21), 2569.
Schlesinger, M.E., Ramankutty, N., 1994. An oscillation in the global climate system of period 65–70 years. Nature 367, 723–726. https://doi.org/10.1038/367723a0.
Schrijver, C.J., Livingston, W.C., Woods, T.N., Mewaldt, R.A., 2011. The minimal solar activity in 2008–2009 and its implications for long-term climate modeling. Geophys. Res. Lett. 38, L06701 https://doi.org/10.1029/2011GL046658.
Shaviv, Nir, 2008. Using the oceans as a calorimeter to quantify the solar radiative forcing. J. Geophys. Res. 113. A11101. http://www.sciencebits.com/files/articles/CalorimeterFinal.pdf.
Shindell, D.T., Schmidt, G.A., Mann, M.E., Rind, D., Waple, A., 2001. Solar forcing of regional climate change during the Maunder Minimum. Science 294 (5549), 2149–2152. https://doi.org/10.1126/science.1064363.
Smyth, T.J., 2011. Penetration of UV irradiance into the global ocean. J. Geophys. Res. https://doi.org/10.1029/2011JC007183, 116C11020.
Song, J., Klotzbach, P.J., Duan, Y., 2021. Statistical linkage between coastal El Niño–Southern Oscillation and tropical cyclone formation over the western North Pacific. Atmos. Sci. Lett. https://doi.org/10.1002/asl.1071 e1071.
Spencer, R., 2010. Low Climate Sensitivity Estimated from the 11-Year Cycle in Total Solar Irradiance. http://www.drroyspencer.com/2010/06/low-climate-sensitivity-estimated-from-the-11-year-cycle-in-total-solar-irradiance/. Latest access 1 June 2021.

Suess, H.E., 1980. The radiocarbon record in tree rings of the last 8000 years. Radiocarbon 22, 200–209. https://doi.org/10.1017/S0033822200009462.
Sun, Q., Miao, C., AghaKouchak, A., Duan, Q., 2016. Century-scale causal relationships between global dry/wet conditions and the state of the Pacific and Atlantic Oceans. Geophys. Res. Lett. 43 (12), 6528–6537. https://doi.org/10.1002/2016GL069628.
Tao, L., Duan, W., Vannitsem, S., 2020. Improving forecasts of El Niño diversity: a nonlinear forcing singular vector approach. Clim. Dyn. 55, 739–754. https://doi.org/10.1007/s00382-020-05292-5.
Thomas, Erin, 2017. Modeling a mechanism of El Niño initiation. Research & Technology. https://doi.org/10.1063/PT.5.4028.
Trenberth, K.E., Fasullo, J.T., Balmaseda, M.A., 2014. Earth's Energy Imbalance. J. Clim. 27, 3129–3144. https://doi.org/10.1175/JCLI-D-13-00294.1.
Tsonis, A.A., Deyle, E.R., May, R.M., Sugihara, G., Swanson, K., Verbeten, J.D., Wang, G., 2015. Dynamical evidence for causality between galactic cosmic rays and interannual variation in global temperature. Proc. Natl. Acad. Sci. U. S. A. 112, 3253–3256.
Tunnicliffe, Wilson Granville 2016. Time Series Analysis: Forecasting and Control, 5th Edition, by George E. P. Box, Gwilym M. Jenkins, Gregory C. Reinsel and Greta M. Ljung, John Wiley and Sons Inc., Hoboken, New Jersey, pp. 712. doi.org/10.1111/jtsa.12194.
van Loon, H., Meehl, G.A., Shea, D.J., 2007. Coupled air-sea response to solar forcing in the Pacific region during northern winter. J. Geophys. Res. https://doi.org/10.1029/2006JD007378, 112D02108.
Vaquero, J.M., 2007. Historical sunspot observations: a review. Adv. Space Res. 40, 929–941. https://doi.org/10.1016/j.asr.2007.01.087 arXiv:astro-ph/0702068.
Wang, G., Cheng, L., Abraham, J., Li, C., 2017a. Consensuses and discrepancies of basin-scale ocean heat content changes in different ocean analyses. Clim. Dyn. https://doi.org/10.1007/s00382-017-3751-5.
Wang, G., Yang, P., Zhou, X., 2017b. Identification of the driving forces of climate change using the longest instrumental temperature record. Sci. Rep. 7, 46091. https://doi.org/10.1038/srep46091.
Webb, David J., Coward, Andrew C., Snaith, Helen M., 2020. A comparison of ocean model data and satellite observations of features affecting the growth of the North Equatorial Counter Current during the strong 1997–1998 El Niño. Ocean Sci. 16, 565–574. https://doi.org/10.5194/os-16-565-2020.
White, W.B., Lean, J., Cayan, D.R., Dettinger, M.D., 1997. Response of global upper ocean temperature to changing solar irradiance. J. Geophys. Res. 102 (C2), 3255–3266. https://doi.org/10.1029/96JC03549.
Wolter, K., Timlin, M.S., 1993. Monitoring ENSO in COADS with a seasonally adjusted principal component Index. In: Proceedings of the 17th Climate Diagnostics Workshop, 52–57, Norman, OK.
Wolter, K., Timlin, M.S., 1998. Measuring the strength of ENSO events – how does 1997/98 rank? Weather 53, 315–324.
Wolter, K., Timlin, M.S., 2011. El Niño/Southern Oscillation behavior since 1871 as diagnosed in an extended multivariate ENSO Index (MEI.ext). Int. J. Climatol. 31, 1074–1087. https://doi.org/10.1002/joc.2336.
Xiao, Zi-Niu, Li, De-Lin, Zhou, Li-Min, Liang, Zhao, Huo, Wen-Juan, 2017. Interdisciplinary studies of solar activity and climate change. Atmos. Oceanic Sci. Lett. 10 (4), 325–328. https://doi.org/10.1080/16742834.2017.1321951.
Yamakawa, S., Makoto, I., Ramasamy, S., 2016. Relationships between solar activity and variations in SST and atmospheric circulation in the stratosphere and troposphere. Quat. Int. 397, 289–299.
Yang, Q., Majda, A.J., Chen, N., 2021. ENSO diversity in a tropical stochastic skeleton model for the MJO, El Niño, and dynamic walker circulation. J. Clim. 34 (9), 3481–3501. Retrieved May 27, 2021, from. https://journals.ametsoc.org/view/journals/clim/34/9/JCLI-D-20-0447.1.xml.
Yim, B.Y., Noh, Y., Yeh, S.-W., Kug, J.-S., Min, H.S., Qiu, B., 2013. Ocean mixed layer processes in the Pacific Decadal Oscillation in coupled general circulation models. Clim. Dyn. 41, 1407–1417. https://doi.org/10.1007/s00382-012-1630-7.
Yoon, J., Yeh, S.-W., 2010. Influence of the Pacific Decadal Oscillation on the relationship between El Niño and the Northeast Asian summer monsoon. J. Clim. 23, 4525–4537. https://doi.org/10.1175/2010JCLI3352.1.
Yuan, Y., Yan, H., 2012. Different types of La Niña events and different responses of the tropical atmosphere. Chin. Sci. Bull. 58, 406–415. https://doi.org/10.1007/s11434-012-5423-5.
Zhai, Q., 2017. Evidence for the effect of sunspot activity on El Niño/Southern Oscillation. New Astron. 52, 1–7. https://doi.org/10.1016/j.newast.2016.09.004.
Zhang, Y., Wallace, J.M., Battisti, D.S., 1997. ENSO-like Interdecadal Variability: 1900–93. J. Clim. 10, 1004–1020.
Zhang, T., Hoell, A., Perlwitz, J., Eischeid, J., Murray, D., Hoerling, M., Hamill, T.M., 2019. Towards probabilistic multivariate ENSO monitoring. Geophys. Res. Lett. 46, 10532–10540. https://doi.org/10.1029/2019GL083946.
Zhou, J., Tung, K., 2010. Solar cycles in 150 years of global sea surface temperature data. J. Clim. 23, 3234–3248. http://journals.ametsoc.org/doi/abs/10.1175/2010JCLI3232.1.
Zong, Z., Yong, L., Jian, H., 2014. Effects of sunspot on the multi-decadal climate projections. Adv. Clim. Chang. Res. 5, 51–56. https://doi.org/10.3724/SP.J.1248.2014.051.